

# Experimental investigation on bubble departure diameter in pool boiling under sub-atmospheric pressure

Gao, W.; Qi, J.; Yang, X.; Zhang, J.; Wu, Dawei

DOI:

[10.1016/j.ijheatmasstransfer.2019.01.024](https://doi.org/10.1016/j.ijheatmasstransfer.2019.01.024)

License:

Creative Commons: Attribution-NonCommercial-NoDerivs (CC BY-NC-ND)

*Document Version*

Peer reviewed version

*Citation for published version (Harvard):*

Gao, W, Qi, J, Yang, X, Zhang, J & Wu, D 2019, 'Experimental investigation on bubble departure diameter in pool boiling under sub-atmospheric pressure', *International Journal of Heat and Mass Transfer*, vol. 134, pp. 933-947. <https://doi.org/10.1016/j.ijheatmasstransfer.2019.01.024>

[Link to publication on Research at Birmingham portal](#)

## General rights

Unless a licence is specified above, all rights (including copyright and moral rights) in this document are retained by the authors and/or the copyright holders. The express permission of the copyright holder must be obtained for any use of this material other than for purposes permitted by law.

- Users may freely distribute the URL that is used to identify this publication.
- Users may download and/or print one copy of the publication from the University of Birmingham research portal for the purpose of private study or non-commercial research.
- User may use extracts from the document in line with the concept of 'fair dealing' under the Copyright, Designs and Patents Act 1988 (?)
- Users may not further distribute the material nor use it for the purposes of commercial gain.

Where a licence is displayed above, please note the terms and conditions of the licence govern your use of this document.

When citing, please reference the published version.

## Take down policy

While the University of Birmingham exercises care and attention in making items available there are rare occasions when an item has been uploaded in error or has been deemed to be commercially or otherwise sensitive.

If you believe that this is the case for this document, please contact [UBIRA@lists.bham.ac.uk](mailto:UBIRA@lists.bham.ac.uk) providing details and we will remove access to the work immediately and investigate.

# Experimental investigation on bubble departure diameter in pool boiling under sub-atmospheric pressure

Gao, Wenzhong; Qi, Jiaye; Yang, Xuan; Zhang, Jiahao; Wu, Dawei

DOI:

[10.1016/j.ijheatmasstransfer.2019.01.024](https://doi.org/10.1016/j.ijheatmasstransfer.2019.01.024)

License:

Creative Commons: Attribution-NonCommercial-NoDerivs (CC BY-NC-ND)

*Document Version*

Peer reviewed version

*Citation for published version (Harvard):*

Gao, W, Qi, J, Yang, X, Zhang, J & Wu, D 2019, 'Experimental investigation on bubble departure diameter in pool boiling under sub-atmospheric pressure', *International Journal of Heat and Mass Transfer*, vol. 134, pp. 933-947. <https://doi.org/10.1016/j.ijheatmasstransfer.2019.01.024>

[Link to publication on Research at Birmingham portal](#)

## General rights

Unless a licence is specified above, all rights (including copyright and moral rights) in this document are retained by the authors and/or the copyright holders. The express permission of the copyright holder must be obtained for any use of this material other than for purposes permitted by law.

- Users may freely distribute the URL that is used to identify this publication.
- Users may download and/or print one copy of the publication from the University of Birmingham research portal for the purpose of private study or non-commercial research.
- User may use extracts from the document in line with the concept of 'fair dealing' under the Copyright, Designs and Patents Act 1988 (?)
- Users may not further distribute the material nor use it for the purposes of commercial gain.

Where a licence is displayed above, please note the terms and conditions of the licence govern your use of this document.

When citing, please reference the published version.

## Take down policy

While the University of Birmingham exercises care and attention in making items available there are rare occasions when an item has been uploaded in error or has been deemed to be commercially or otherwise sensitive.

If you believe that this is the case for this document, please contact [UBIRA@lists.bham.ac.uk](mailto:UBIRA@lists.bham.ac.uk) providing details and we will remove access to the work immediately and investigate.

# Experimental investigation on bubble departure diameter in pool boiling under sub-atmospheric pressure

Wenzhong Gao<sup>1,3</sup>, Jiaye Qi<sup>1</sup>, Xuan Yang<sup>1</sup>, Jiahao Zhang<sup>1</sup>, Dawei Wu<sup>2</sup>

(1. Merchant Marine College, Shanghai Maritime University, Shanghai, 201306, China; 2. School of Marine Science and Technology, Newcastle University, Newcastle upon Tyne, NE1 7RU, United Kingdom; 3. College of energy engineering, ZheJiang University, Hangzhou, 310058, China)

---

## Abstract

The objective of this research is to compare the nucleate boiling characteristic of the calcium chloride aqueous solution with distilled water at sub-atmospheric pressure by analyzing the growing bubble dynamics in order to provide some data for optimizing the design of the dehumidification system. The experiments were carried out with water and calcium chloride solution on the upper surface of a polished stainless steel plate, under sub-atmospheric pressure ranging from 3.6kPa to 22.0kPa. An artificial nucleation site was created in the center of the plate to generate the isolated bubbles. A high-speed camera was used to capture the images of dynamic bubbles, and the relevant parameters on bubble dynamics were measured and calculated by frame-by-frame image treatment.

Experimental results show that bubble diameter tends to increase with the pressure decrease which means the lower vapor density and stronger surface tension force at sub-atmospheric boiling. The influence of superheat and sub-cooling degree were also analyzed. Additionally, a complex boiling regime of calcium chloride solution with irregular bubble dynamic parameters was observed. Finally, bubble growth dynamics under sub-atmospheric were analyzed and the force balance equation were established. It is shown that the dynamic effect especially the inertial force dominated the growth stage under sub-atmospheric boiling. A new bubble departure diameter correlation within  $\pm 20\%$  deviation was proposed.

29 *Keywords:* nucleate pool boiling; sub-atmospheric pressure; bubble departure  
 30 diameter; [calcium chloride aqueous solution](#)

Nomenclature	$P_v$	the vapor pressure (Pa)
AAD the average absolute deviation (%)	Pr	Prandtl number, $Pr = \nu/\alpha$
AD the average deviation (%)	q	heat flux ( $\text{kW m}^{-2}$ )
Ar Archimedes number, $Ar = [g\rho_l(\rho_l - \rho_v)/\mu_l^2][\sigma/g(\rho_l - \rho_v)]^{3/2}$	R	bubble radius (m)
a the length of the semi-minor axis (m)	$T_{sat}$	the saturation temperature( $^{\circ}\text{C}$ )
b the length of the semi-major axis (m)	$T_w$	the heated wall temperature( $^{\circ}\text{C}$ )
	$T_s$	the saturation temperature( $^{\circ}\text{C}$ )
C a parameter in fritz correlation	$t_g$	bubble growth period (s)
$c_p$ specific heat capacity (J/kg)	$t_w$	bubble waiting period (s)
$D_d$ bubble departure diameter (mm)	$\Delta T$	surface superheat (K)
$D_{eq}$ the equivalent bubble diameter (mm)	$P_{\infty}$	<a href="#">ambient pressure(Pa)</a>
	$P_{wall}$	<a href="#">the heated wall pressure(Pa)</a>
$F_b$ buoyancy force (N)		
$F_i$ inertial force (N)		
$F_M$ Maragoni force (N)		
$F_p$ pressure force (N)		
$F_s$ surface tension force (N)		
f the bubble departure frequency (Hz)		
g gravitational acceleration ( $\text{ms}^{-2}$ )		
$h_l$ the liquid height (cm)		
	Greek letters	
$g_c$ gravitational acceleration correction factor	$\alpha$ ( $\text{m}^2\text{s}^{-1}$ )	thermal diffusivity
$h$ the heat transfer coefficient ( $\text{kW m}^{-1}\text{K}^{-1}$ )	$\theta$	contact angle, deg
$h_{lv}$ latent heat (J/kg)	$\mu$	dynamic viscosity (Pa s)
Ja Jacob number, $Ja = \rho_l c_p \Delta T / \rho_v h_{lv}$	$\rho_l$	liquid density ( $\text{kg m}^{-3}$ )

$K_1$	a parameter defined by Jensen and Memmel [20], $K_1 = (Ja/Pr)^2(Ar)^{-1}$	$\rho_v$	vapor density ( $\text{kg m}^{-3}$ )
L	the calibrated length of the ruler (m)	$\sigma$ ( $\text{N m}^{-1}$ )	surface tension coefficient
P	pressure (Pa)	$\xi$	the Maragoni correlation factor

## 31 1.Introduction

32 In recent years, due to new environmental restrictions and ever-increasing demand  
33 of energy efficiency, absorption refrigerating plants and liquid desiccant  
34 dehumidification systems has become more and more popular. In such systems,  
35 nucleate boiling is a widely used method of regeneration due to its high heat transfer  
36 coefficient between solid and liquid. Bubble growth and detachment processes have a  
37 major impact on nucleate boiling heat transfer. A bubble growth cycle includes:  
38 (1)Nucleation period, a bubble nucleates from a single site on the heating  
39 surface;(2)Growing period, the bubble grows larger over time, during this period, the  
40 convection between liquid and wall is enhanced because of the hot capillary action in  
41 vapor-liquid interface;(3)Departure period, when the bubble grows to a certain size, it  
42 will depart from the surface, at the same time, liquid with lower temperature will flow  
43 into the area that the bubble used to be, so that the wall will be cooled instantly and a  
44 lot of heat will be exchanged. It is believed that the nucleation boiling heat transfer is  
45 directly influenced by the bubble detachment, so both of the bubble departure  
46 diameter and the bubble departure frequency are important parameters that need to be  
47 conveyed.

48 Compared with the boiling heat transfer at atmospheric pressure, it has been found  
49 that the boiling heat transfer is deteriorated with lower heat transfer coefficient [1] and  
50 larger temperature fluctuations [2-3] at sub-atmospheric pressure. However, only a  
51 few studies [2,4-8] on pool boiling at sub-atmospheric pressures have directly  
52 characterized bubble formation, growth and dynamic behavior, and developed the  
53 correlations for bubble dynamics. The lack of work is partly due to the complexity of  
54 the boiling environment at sub-atmospheric pressure. In sub-atmospheric boiling,  
55 bubble behavior is quite different from that at the atmospheric conditions. Large  
56 non-spherical bubbles, long waiting period, the non-homogeneous boiling  
57 environment [5] indicate that traditional models do not apply in the sub-atmospheric  
58 conditions. It's also difficult to isolate an individual influencing factor, since the

59 different phenomenon in sub-atmospheric pool boiling is a result of the combined  
60 effects of various factors.

61 One of the early sub-atmospheric pool boiling experiments was conducted by  
62 Yagov et al. [4]. The results of boiling of water, ethyl alcohol and NaCl solution  
63 under low pressures were presented. Extremely long period in vapor formation,  
64 millimeters-sized bubbles and severe perturbation of the liquid were observed during  
65 the experiment. Van Stralen et al. [2] discovered the bubble growth rates of water and  
66 organic component at sub-atmospheric pressures. They found that both the bubble  
67 growth time and departure radius increase with decreasing pressure. “Rayleigh”  
68 bubbles and a high-velocity liquid jet were observed under the low pressure, which  
69 was attributed to the occurrence of dry area according to their theory. Giraud et al. [5]  
70 pointed out that it was the non-homogeneity environment that results in the different  
71 phenomena in the sub-atmospheric pool boiling. The instantaneous boiling curves  
72 were presented and a particular “cyclic boiling regime” was investigated in which  
73 wall temperature fluctuations can reach 20K. It was also highlighted that the liquid  
74 height was an important parameter. Although some typical phenomena were presented  
75 and analyzed, those studies remain qualitative. It is still unclear how the theoretical  
76 correlations of bubble dynamics obtained under atmospheric condition change under  
77 sub-atmospheric conditions. Zajackowski et al. [6] analyzed several correlations for  
78 heat transfer coefficient in sub-atmospheric conditions, and found the most accurate  
79 correlation, but no bubble dynamic parameters were involved. Non-dimensional  
80 characteristic radius and time scale parameters were used by Kim et al. [7] to compare  
81 the difference between bubble growth behavior at atmospheric and sub-atmospheric  
82 pressure. However, the comparison may not be valid because the liquid height was  
83 unknown. Michaie et al. [8] used image processing software to calculate some  
84 quantitative parameters in sub-atmospheric boiling, but no further analysis was  
85 presented. In atmospheric or higher pressure, bubble dynamic parameters and their  
86 correlations with influencing factors are studied by numerous researchers. Bubble  
87 departure diameter and bubble departure frequency are the crucial parameters  
88 referring to bubble dynamics. The correlation proposed by Fritz [9] as shown Eq. (1)  
89 has withstood the test of time and were modified by various researchers. The equation  
90 was based on pure liquid and liquid mixture, where  $\theta$  is the contact angle.

$$91 \quad D_d = 0.0146\theta \sqrt{\frac{2\sigma}{g(\rho_l - \rho_v)}} \quad (1)$$

92 Cole and Rohsenow [10] have modified the Fritz correlation by involving heat flux  
 93 appearing in Jacob number.

$$94 \quad D_d = CJa^{\frac{5}{4}} \left[ \frac{2\sigma g_c}{g(\rho_l - \rho_v)} \right]^{\frac{1}{2}} \quad (2)$$

95 Other mostly used correlations in previous studies are presented in Table 1. All of  
 96 the correlations were obtained from Mohanty et al. [11]. Those correlations worked  
 97 well in their experiments, but it is still unknown whether these correlations can predict  
 98 well under sub-atmospheric boiling conditions.

99 **Table 1**

100 Bubble departure diameter and frequency correlations

$D_d = 0.02080 \left[ \frac{\sigma g_c}{g(\rho_l - \rho_v)} \right]^{1/2} \left[ 1 + 0.0025 \left( \frac{dD}{dt} \right)^{\frac{3}{2}} \right]$	Cole and Shulman[12]
$D_d = 0.04Ja \left[ \frac{2\sigma}{g(\rho_l - \rho_v)} \right]^{1/2}$	Cole[13]
$D_d = 0.25(1 + 10^5 K_1)^{1/2} \left[ \frac{\sigma g_c}{g(\rho_l - \rho_v)} \right]^{1/2}$	Kutateladeze and Gogonon[14]
For $K_1 < 0.06$ , where $K_1 = \left( \frac{Ja}{Pr_l} \right)^2 (Ar)^{-1}$	
$D_d = 0.19(1.8 + 10^5 K_1)^{2/3} \left[ \frac{\sigma}{g(\rho_l - \rho_v)} \right]^{1/2}$	Jensen and Memmel[15]
$D_d = 0.1649Ja^{0.7} \left[ \frac{\sigma g_c}{g(\rho_l - \rho_v)} \right]^{1/2}$	Kim and Kim[16]

101 Though so many researches have been done to investigate bubble departure  
 102 mechanisms, study about binary mixtures and correlations to predict bubble departure  
 103 diameter still arises wide interest. In this work, calcium chloride aqueous solution is  
 104 used as the working fluid to improve our research on dehumidification system  
 105 regeneration and also to make a thermo-physical properties comparison with distilled  
 106 water under the influence of sub-atmospheric pressure. The experiment was  
 107 conducted on the upper surface of a smooth stainless-steel plate heated by a controlled  
 108 oil bath. High speed visualization technology was used to monitor the boiling surface,  
 109 and image processing software was used to extract data. The influence of pressure,  
 110 superheat, and subcooling degree were presented. Meanwhile, bubble dynamics  
 111 behavior and force balance were analyzed. Since most of the empirical correlations  
 112 used in the system design are based on data at atmospheric pressure, by analyzing  
 113 experimental phenomena, experimental data, and by force analysis, a new correlation  
 114 suitable for predicting the bubble departure diameter of water and binary mixtures  
 115 under sub-atmospheric temperature is proposed.

## 116 **2.Experimental**

### 117 **2.1 Setup**

118 The schematic experimental apparatus of pool boiling are shown in Fig.1. The  
119 boiling vessel was constituted by two stainless steel blind plates (diameter 160mm)  
120 and a toughened glass cylinder with 90mm inner diameter and 200mm height. They  
121 were held together by four bolts and nuts. O-rings seals were placed between the two  
122 blind plates and the glass cylinders with the aim of pledging gas-tightness. The vessel  
123 was evacuated through a valve connected to a vacuum pump at the top of the upper  
124 blind plate. The vapor was condensed through another valve connected to a condenser  
125 in order to recycle the evaporated working liquid. Due to the need of frequent  
126 assembly and disassembly as well as high gas-tightness, all components of the  
127 experimental facilities were made in vacuum technology (ISO-KF).

128 A stainless steel ruler with the length of 150mm was placed inside the glass  
129 cylinder as the reference length to measure the liquid height and bubble size. Two  
130 K-type thermocouples were embedded in the upper blind plate and sealed by sealant.  
131 They were used to measure the vapor and the liquid temperatures. Another four  
132 K-type thermocouples were embedded into the lower blind plate close to the heating  
133 surface to evaluate the heat flux with the help of Fourier's law. The calculation of the  
134 heat flux and its uncertainty was based on the work of Gong et al. [17]. A fast  
135 response thermocouple was placed on the upper surface to measure the instantaneous  
136 wall temperature. A pressure transducer with range of 0–20 kPa was used to measure  
137 the vapor pressure. Agilent data logger was used to record temperatures, pressures and  
138 heat flux. The uncertainties of the measurement instruments are summarized in Table  
139 2.

140 The experiments were carried out on the upper surface of the lower blind plate. The  
141 surface of the stainless steel blind plate was polished with the measured roughness of  
142  $0.4\mu\text{m}$ . An artificial nucleation site with the diameter of  $150\mu\text{m}$  and depth of  $70\mu\text{m}$   
143 [18]was created at the center of the blind plate. The boiling vessel was heated by a  
144 controlled oil bath containing silicone oil. During the experiment the oil temperature  
145 was set to a constant value in order to maintain a constant given temperature.

146 A high speed camera was placed near the glass cylinder to capture the pictures of  
147 bubbles growth, detachment and breakup. The camera highest acquisition frequency is



148 1000fps and the resolution is 800×600 pixels. A halogen backlight device was placed  
149 in the opposite position to illuminate the boiling area. The 150W halogen lamp can  
150 produce intense and homogeneous light to make a decent contrast for clear analysis.  
151 The images were analyzed by AOS Imaging Studio software to get the bubble  
152 departure diameters. From the captured images, a physical dimension of 90 mm  
153 corresponds to 354 pixels, leading to 0.254 mm per pixel. An image processing  
154 software was used to measure the contact angle through analyzing the images, as  
155 shown in Fig. 2. The contact angle values of water and calcium chloride solution are  
156 35.36 degrees and 32.29 degrees, respectively. As each photo has its own  
157 time-stamp, bubble growth period and bubble waiting period can be calculated by  
158 finding the creation and detachment frame during a frame-by-frame treatment.

## 159 **2.2 Determination of the bubble equivalent diameter**

160 Under sub-atmospheric pool boiling conditions, the bubble shape is no longer  
161 sphere. In our experiment, a flattened spheroid shaped bubble was observed as shown  
162 in Fig. 3a, which is in agreement with Ref [4, 8]. The geometry of a flattened spheroid  
163 is shown in Fig. 3b.

164 As shown in Fig. 3a, the spheroid shape is almost axis-symmetric and a bit  
165 non-symmetric in the vertical direction. Therefore, neither of the equatorial diameters  
166 3a nor 3b shown in Fig. 3b can be a good sample of the equivalent diameter. In most  
167 previous studies, researchers used the equivalent diameter of a sphere with the same  
168 volume. So the bubble equivalent diameter can be calculated as in Eq. (3),

$$169 \quad D_{eq} = 2\sqrt{ab} \quad (3)$$

## 170 **2.3 Experimental uncertainty**

171 As mentioned above, the geometry length of bubbles was measured by counting  
172 pixels in a captured image. The error of the measurement is of ±2 pixels at the  
173 beginning of the growth and ±1 pixels at the end of the growth and the uncertainty of  
174 the bubble diameter is ±2.6%. The error of the measurement of contact angle is ±1  
175 degree.

176 Due to the vacuum environment and good insulation measures, an adiabatic  
 177 condition can be obtained. According to the Fourier Law, heat flux can be calculated  
 178 by Eq. (4):

$$179 \quad q_i = \lambda_i (T_i - T_{i-1}) / (x_i - x_{i-1}) \quad (4)$$

180 Where  $x_i$  is the distance between corresponding measurement point and the heating  
 181 surface,  $i=1,2,3,4$ , as shown in Fig. 4;  $T_i$  is the temperature,  $\lambda_i$  is the average thermal  
 182 conductivity of stainless steel between the  $i-1$  point and  $i$  point.

183 The average heat flux is:

$$184 \quad q = \frac{1}{3} \left\{ \sum_{i=1}^3 [\lambda_{i+1} (T_{i+1} - T_i) (x_{i+1} - x_i)] \right\} \quad (5)$$

185 According to the Taylor experimental error analysis formula, synthetic standard  
 186 uncertainty (U) is calculated by standard uncertainty ( $u_i$ ). Since all temperatures are  
 187 measured by thermocouples whose precision is  $\pm 0.1\text{K}$ , the temperature uncertainty is:

$$188 \quad u(T) = \sqrt{\left[ \frac{\partial(T)}{\partial x_1} u(x_1) \right]^2 + \left[ \frac{\partial(T)}{\partial x_2} u(x_2) \right]^2 + \left[ \frac{\partial(T)}{\partial x_3} u(x_3) \right]^2} \quad (6)$$

189 For the length measurement, the standard deviation of ten times length  
 190 measurements is obtained as:

$$191 \quad u(\bar{x}_i) = \sqrt{\frac{1}{n(n-1)} \sum_{i=1}^n (l_i - \bar{l})^2} \quad (7)$$

192 So the uncertainty of heat flux can be expressed as:

$$193 \quad u(q) = \sqrt{\left[ \frac{\partial f(q)}{\partial T_1} u(T_1) \right]^2 + \left[ \frac{\partial f(q)}{\partial T_2} u(T_2) \right]^2 + \left[ \frac{\partial f(q)}{\partial T_3} u(T_3) \right]^2 + \left[ \frac{\partial f(q)}{\partial T_4} u(T_4) \right]^2 + \left[ \frac{\partial f(q)}{\partial l_1} u(l_1) \right]^2 + \left[ \frac{\partial f(q)}{\partial l_2} u(l_2) \right]^2 + \left[ \frac{\partial f(q)}{\partial l_3} u(l_3) \right]^2 + \left[ \frac{\partial f(q)}{\partial l_4} u(l_4) \right]^2} \quad (8)$$

## 194 2.4 Procedure and operating conditions

195 Since the experiments need to be implemented under sub-atmospheric pressure, a  
 196 high level of gas-tightness is required. The entire system, including the condenser and  
 197 the vacuum pump were cleaned and tested before the experiments. After the test  
 198 solution was prepared and pipetted into the boiling vessel through a valve, the vacuum

199 pump was then turned on. When the pressure of the system was stabilized and the  
200 dissolved gases were released from the solution, the controlled oil bath was switched  
201 on to heat the boiling vessel allowing the saturation temperature of the solution to be  
202 reached. Meanwhile, the condenser was turned on to keep the system pressure from  
203 rising by condensing the vapor. After the system reached a steady state, the  
204 high-speed camera and the halogen lamp were turned on. The visual information as  
205 well as the experimental parameters including the surface temperature( $P_{wall}$ ), the  
206 liquid temperature( $\rho gh$ ) and the system pressure( $P_v$ ) were collected and recorded in a  
207 PC-based data acquisition system.

208 The experiments were conducted with distilled water and calcium chloride aqueous  
209 solution. Reagents and distilled water were used to prepare the experimental solution  
210 analytically. Distilled water was used in the first set of experiment for eight values of  
211 vapor pressure  $P_v$  starting from 3.6 kPa up to 22.0 kPa. The liquid height was set as a  
212 constant value of  $H_l = 15.0\text{ cm}$  for all sets of experiments. The controlled oil bath  
213 was set with different oil temperature in each set of experiment to discover the  
214 relationship between wall temperature and bubble parameters. Calcium chloride  
215 aqueous solution was conducted in the second set of experiments with the same liquid  
216 height. Moreover, in order to provide some basic data for future research on  
217 promoting the application of low-grade waste heat in solution dehumidification  
218 system, five values of vapor pressure  $P_v$  starting from 4.2 kPa up to 20.0 kPa were  
219 adopted. The full operating conditions and selected physical properties of the  
220 experimental solution are presented in Table 3.

## 221 **3.Results and discussion**

### 222 **3.1 Bubble growth cycle at different sub-atmospheric pressure**

#### 223 **3.1.1 Boiling environment**

224 Since the experiment was conducted at pressure ranges from 3.6kPa to 22kPa and  
225 the working fluids including water and calcium chloride solution, the boiling  
226 environment is non-homogeneous mainly due to the following reasons. First, the  
227 pressure generated by the liquid height may be in the same order of magnitude as the  
228 fluid saturation pressure, which means different liquid height leads to different  
229 pressure, as a result, the pressure and saturation temperature of the working fluid can

230 be highly non-homogeneous[2];Secondly, the different properties of the components  
231 in the binary system result in different boiling characteristics, which leads to  
232 concentration gradient and temperature gradient starting from the heated surface, the  
233 concentration gradient and temperature gradient therefore, strengthen inhomogeneity.  
234 Generally speaking, the pressure gradient, concentration gradient and temperature  
235 gradient leads to the special boiling environment at sub-atmospheric pressure, as well  
236 as the non-homogeneity on bubble growth and shape.

### 237 **3.1.2Boiling phenomena analysis**

238 In sub-atmospheric pressure, both the bubble size and shape are quite different from  
239 those under the atmospheric conditions. The bubble life cycle of distilled water in 4.2  
240 kPa and 22.0kPa is shown in Fig. 5a. As shown in this figure, at  $P_v = 4.2$  kPa a  
241 bubble nucleates in the artificial nucleation site on the boiling surface and grows with  
242 a hemi-sphere shape during the initial 10ms. Then, the bubble is prolonged into a  
243 centimeter-sized spheroid shape before detachment. A liquid jet was observed  
244 penetrating the lower side of the bubble before the bubble collapses. At  $P_v = 20$  kPa,  
245 a bubble of the similar shape with the lower pressure was observed, but it was much  
246 smaller in size. When the bubble is about to depart, the secondary bubble penetrated  
247 the first one and a mushroom shape was observed. The phenomena were similar with  
248 those observed by previous studies [2,4,5,8]. According to Van Stralen [2], the  
249 high-velocity liquid jet in 4.2kPa is owing to the liquid depression after the primary  
250 bubble departs and the formation of the mushroom shape is due to the dry area  
251 beneath the center of the first bubble. The author compared this behavior to film  
252 boiling because of the low value thermal-conductivity of the vapor.

253 The bubble growth curves of distilled water at different pressure are shown in Fig.  
254 6a. Take  $P_v = 4.2$ kPa for example, the initial 40ms can be recognized as the rapid  
255 growth period in which the liquid inertia and surface tension force governs. From  
256 40ms to the time that bubble departs, the thermal diffusion dominates the growing  
257 process during which bubble grows at slow speed. Comparing the curves at different  
258 pressure, it's obvious that with the increase of the pressure level, both the bubble  
259 equivalent diameter and bubble growth time decreases. According to Michae [8], this  
260 is because the vapor density  $\rho_v$  grows rapidly with the decrease of pressure while the  
261 liquid density  $\rho_l$  is basically unchanged. Hence, vaporizing certain mass of liquid

262 require a much larger vapor volume in lower pressure than higher pressure. Surface  
263 tension force also increases with the decrease of pressure resulting in the difficulty in  
264 the bubble detachment and induces a longer bubble growth time. In general, the  
265 analysis mentioned above shows that our experimental method and procedure was  
266 verified to be appropriate.

267 The typical bubble shape of calcium chloride aqueous solution in different pressure  
268 is shown in Fig. 5b. Analogously, bubbles of spheroid shape were observed. In lower  
269 pressure, large bubbles and high liquid jet were also observed. Owing to the relatively  
270 high saturation temperature, there is absence of mushroom bubble in 20kPa which  
271 leads to the diminution of the dry area and liquid depression.

272 The boiling phenomenon of aqueous salt solution can be quite different from the  
273 boiling of distilled water based on the following reasons. First, the thermo-physical  
274 properties of the salt solution are different from distilled water. The change in  
275 saturation pressure, contact angle and surface tension force leads to different boiling  
276 characteristics. Secondly, the salt solution belongs to the binary systems, which is  
277 different from the pure liquid. During the boiling transfer, the light component in the  
278 solution near the heated surface is boiled at first. As the boiling continues, the  
279 concentration of the solution near the heated surface is increased, which leads to the  
280 change of physical properties near the heated surface.

## 281 **3.2 Bubble departure diameter and frequency at different sub-atmospheric** 282 **pressure**

### 283 **3.2.1 Bubble departure diameter and frequency of distilled water**

284 Fig. 6b shows the relationship between bubble departure diameter and pressure of  
285 distilled water. It's clear that the bubble departure diameter increases as pressure  
286 decreases. At the lowest pressure ( $P_v = 4.2\text{kPa}$ ), bubble departure diameter can reach  
287 85mm while at higher pressure ( $P_v = 20\text{kPa}$ ) the bubble size is much smaller. As  
288 mentioned above, vapor density and surface tension force is the main reason behind  
289 this phenomenon. In fact, in most bubble departure diameter correlations, the bubble  
290 diameter is proportional to Ja number. As the pressure decreases, vapor density  $\rho_v$   
291 increases, which results in the larger size bubble at lower pressure.

292 The bubble waiting time and frequency at different pressure of distilled water are  
293 shown in Fig. 6c. Bubble waiting time is defined as the time interval between the first  
294 departing bubbles to the initiation of the successive bubble from the same nucleating

295 cavity. In the range from 3.6kPa to 22.0kPa, the bubble waiting time decreases from  
296 8s to 0.2s. As a result, bubble departure frequency, defined as the reciprocal of the  
297 sum of the bubble waiting time and growth time, increases from 0.1Hz to 4Hz. The  
298 long waiting time in the lower pressure conditions is owing to the large size bubbles.  
299 The detachment of a bubble of that size leads to strong movement in the surrounding  
300 fluid. The liquid near the heating surface is then cooled to approximately the  
301 saturation temperature, which need a lot of time to be re-heated to reach the  
302 nucleation temperature. As for the mushroom shape(the secondary bubble penetrated  
303 the first one) appeared at 20kPa,as shown in Fig. 6e, $t_1$  is the waiting time between the  
304 first bubble and the second one,  $t_2$  is the waiting time between the first bubble and  
305 next first bubble, and  $t_3$  is the waiting time between the mushroom and the next  
306 mushroom .Considering  $t_1$  is small and the secondary bubble is unstable because it is  
307 triggered by the jet flow , so we usually use  $t_2$  as the waiting time, as shown in Fig. 6c.

308 A comparison between experimental data and literature data was made, as shown in  
309 Fig. 7 [3].Considering the difference of working condition and methods, the error of  
310 departure diameter at the same pressure is almost within 20%,which means the results  
311 of this experiment are accurate.

### 312 **3.2.2 Comparison with bubble departure diameter and frequency of distilled** 313 **water and calcium chloride solution**

314 The comparison of the bubble departure diameter and frequency is shown in Fig. 8a.  
315 It can be found that the boiling of calcium chloride solution at sub-atmospheric  
316 pressure is particularly irregular especially in higher pressure conditions. The irregular  
317 departure diameter and frequency reflect the complexity of the boiling conditions of  
318 salt solution at sub-atmospheric pressure. In sub-atmospheric pressure, the  
319 temperature gradient, pressure gradient and the concentration gradient create a volatile  
320 and complex boiling condition. Moreover, the surface tension gradient can be formed  
321 by the concentration gradient, which leads to Marangoni flow. The liquid motions  
322 caused by preceding bubbles and the size of the previous bubble also have effect on  
323 bubble dynamic parameters. This multi-factor combined effect leads to the irregular  
324 departure diameter and frequency. Therefore, it is reasonable to compare the overall  
325 trend rather than single bubble parameters. Overall speaking, comparing water in the  
326 same pressure, the bubble departure diameter of the calcium chloride aqueous solution  
327 decreased and the departure frequency increased. Although the increase of the surface

328 tension force make the bubble harder to detach from the heating surface resulting in  
 329 longer waiting time and larger bubble diameter. The saturation temperature of the  
 330 calcium chloride aqueous solution is higher than water in the same pressure, which  
 331 leads to smaller vapor density. As a result, the bubble departure diameter decreases  
 332 and the bubble departure frequency increases.

333 Fig. 8b shows the bubble departure diameter and frequency in different  
 334 concentration. As shown in Fig. 8b, the irregular distributions still occur in higher  
 335 concentration. It can be concluded that with the increase of concentration, the bubble  
 336 departure diameter decreases and the bubble departure frequency increases. The  
 337 smaller vapor density and stronger Marangoni flow is the reason behind these  
 338 changes.

### 339 **3.3 The effect of wall superheat and subcooling degree at sub-atmospheric** 340 **boiling**

341 Large wall temperature fluctuation was observed during bubbles grew and detach  
 342 process, which is in agreement with Ref [3, 4, 5]. Therefore, the compared wall  
 343 superheat is defined in Eq. (5) as

$$344 \quad \Delta T = T_w(t) - T_{sat}^*, \quad T_S^* = 17.834 \ln P_{wall} - 116.62$$

$$345 \quad P_{wall} = P_{sat} + \rho g h \tag{9}$$

346 where  $T_w(t)$  is the wall temperature when the nucleation begins and  $T_S^*$  is the  
 347 saturation temperature near the surface. Fig. 9a shows the bubble growth curves in  
 348 different wall superheat. As the wall superheat rises, both the bubble equivalent  
 349 diameter and bubble growth time increases, owing to the thicker thermal boundary  
 350 layer in higher wall superheat [19].

351 The typical bubble growth curve of saturated boiling and subcooled boiling is  
 352 shown in Fig. 9b. As shown in the diagram, with the increase of subcooling degree,  
 353 bubble size decreased which is in agreement with the experimental data of Qiu et al.  
 354 [20] and the simulation results of Dhir et al. [21]. In saturated boiling, liquid has no  
 355 need for absorbing heat from bubbles. While in sub-cooled boiling, as shown in Fig.  
 356 10, the vapor forming the bubbles re-condenses and release heat. With the increase of  
 357 the bubble size, the surface area of condensation becomes larger, which results in the

358 increase of condensation rate. However, due to the limitation of the heat flux, the  
 359 condensation rate is constrained as well as the bubble size. Therefore, subcooling  
 360 degree is a constraint on the bubble departure size. Although Marangoni flow that  
 361 occurs in sub-cooling conditions tends to hinder the departure of the bubbles,  
 362 considering that the saturated bubble diameter is much larger than that under  
 363 sub-cooling conditions, the bubble growth period under saturated boiling is still  
 364 longer than that under sub-cooling conditions at sub-atmosphere.

### 365 3.4 A new bubble departure diameters correlation

#### 366 3.4.1 Comparisons of several correlations for bubble departure diameter

367 Although the typical bubble shape was observed and the influence with some  
 368 experimental parameters was summarized, the effects of thermal diffusion, dynamic  
 369 and non-homogeneous environment in sub-atmospheric pressures still need to be  
 370 determined. The experimental data was compared with different bubble growth  
 371 theories and correlations to examine the relative importance of these effects.

372 One of the foremost bubble growth correlations were proposed by Plesset and  
 373 Zwick [22] as in Eq. (10). By neglecting the surface tension force and dynamic  
 374 effects, the bubble growth is only limited by the thermal diffusion process.  
 375 Accordingly, the solution predicts the instantaneous bubble radius for thermal  
 376 diffusion dominated growth. The thermal diffusion controlled growth solutions  
 377 proposed by Plesset and Zwick [22] as well as Forster and Zuber [23] and others are  
 378 in satisfactory agreement with the experimental data in atmospheric and higher  
 379 pressures. However, according to Cole and Shulman [12] the heat diffusion limited  
 380 theory failed to predict the situation under sub-atmospheric conditions. On the other  
 381 hand, the well-known extended Rayleigh [24] equation as shown in Eq. (11) is based  
 382 on an equilibrium balance from the dynamic point of view.

$$383 \quad D=3.908Ja\sqrt{\alpha_1 t} \quad (10)$$

$$384 \quad \frac{P_v(T_v)-P_\infty}{\rho_1} = R \frac{d^2R}{dt^2} + \frac{3}{2} \left( \frac{dR}{dt} \right)^2 + \frac{2\sigma}{\rho_1} \quad (11)$$

385 As is illustrated in Fig. 11, when the pressure was about 20kPa and the Jakob  
 386 number approximately equaled to 267, the theoretical curves lay above the  
 387 experimental data. With the pressure being reduced to 7.3kPa and the Jakob number



388 equaled to 662, the deviation of the Plesset and Zwick correlation became larger. In  
 389 the lowest pressure 4.2kPa and the highest Jacob number 1786, the experimental data  
 390 in the early growing stage coincided with the Rayleigh curves, while the Plesset and  
 391 Zwick correlation didn't predict well in this situation. These comparisons indicate that  
 392 the early growth stage of bubble growth process under sub-atmospheric pressures is a  
 393 significant inertia controlled region.

### 394 **3.4.2 The force balance of the bubble under sub-atmospheric pressure**

395 In order to discover the dynamic behavior and obtain a useful bubble growth model  
 396 under sub-atmospheric pressure, it's important to identify which of the acting forces  
 397 are dominant. The force balance of the isolated bubble is presented in this chapter to  
 398 further analyze the influences of each force under sub-atmospheric pressure. As is  
 399 mentioned above, the flattened spheroid shape is the typical shape of an isolated  
 400 bubble under sub-atmospheric boiling conditions. The geometric parameters and force  
 401 analysis of an isolated bubble is shown in Fig. 12a.

402 Generally speaking, buoyancy force  $F_b$  and pressure force  $F_p$  are the positive  
 403 forces are those tend to push the vapor bubble on to the heating surface. While the  
 404 drag force  $F_d$ , surface tension force  $F_s$ , the Marangoni force  $F_M$  and inertial force  $F_i$   
 405 are the negative forces that prevent bubbles from departing from the heating surface.

406 As a result, the expression of forcer balance is presented in Eq.(12):

$$407 \quad F_b + F_p = F_M + F_s + F_i + F_d \quad (12)$$

408 The expressions of each force are:

409 1. Buoyancy force  $F_b$  is caused by the movement of the fluid due the non-uniform  
 410 density.

$$411 \quad F_b = \frac{4}{3} \pi R_{eq}^3 g (\rho_l - \rho_v) \quad (13)$$

412 2. Pressure force  $F_p$  is the contact capillary pressure force caused by the surface  
 413 tension in the solid-liquid interface.

$$414 \quad F_p = \pi R_c^2 \frac{2\sigma}{R_{eq}} \quad (14)$$

415 3. The inertial force  $F_i$  is deduced by the velocity of the bubble and the volume  
416 expansion.

$$417 \quad F_i = \frac{d}{dt}(m_i v) \quad (15)$$

418 4. The Maragoni force  $F_M$  is caused by surface tension gradient in the vapor-liquid  
419 interface. In atmospheric conditions the surface tension gradient is mainly caused by  
420 temperature gradient. However, in sub-atmospheric conditions the pressure gradient  
421 should not be neglected.

$$422 \quad F_M = \xi_t \frac{d\sigma}{dt} \Delta T + \xi_p \frac{d\sigma}{dt} \Delta p \quad (16)$$

423 5. The surface tension force  $F_s$  acts on the vapor-liquid interface is shown in  
424 Eq.15

$$425 \quad F_s = 2\pi R_c \sigma \sin \theta \quad (17)$$

426 The relationship between the forces acting on the isolated bubble and the bubble  
427 radius was presented in Fig. 12b and Fig 12c. As can be seen from the curves, in  
428 sub-atmospheric boiling conditions, the buoyancy force  $F_b$  and inertial force  $F_i$  are  
429 obviously the dominant forces. Due to the low vapor density in lower pressure, the  
430 large volume of bubbles leads to the exponential growth of the buoyancy and inertial  
431 force compared to the situation in atmospheric pressures. On the other hand, the  
432 influence of the other three forces is relatively small and can be neglected in the  
433 sub-atmospheric pressure. The curves also concurs with the comparison result in the  
434 previous chapter that the inertial forces are the major factor that hinders the bubble  
435 detachment.

436 The results also indicate that the bubble departure diameter correlations such as  
437 Fritz correlations based on the static force balance of the buoyancy and surface  
438 tension force may not be valid under sub-atmospheric pressure. Considering the  
439 significant inertia controlled region, an attempt should be made to find a new  
440 correlation in the sub-atmospheric pool boiling conditions.

### 441 3.4.3 New correlation

442 As is mentioned above, in sub-atmospheric pressures, the initial force is the  
443 dominant negative force. As a result, the force balance equation can be written below,

444 
$$g(\rho_l - \rho_v)V(t_g) = \frac{d}{dt_g}(m_l v) \quad (18)$$

445 where  $V(t_g)$  is the volume of the bubble.

446 Assume that the equivalent bubble diameter  $D_{eq} \propto t_g^n$ ,  $\rho_v \ll \rho_l$  and  $v = \frac{dh}{dt_g}$ ,

447 the Eq.18 can be rewritten as:

448 
$$\frac{d}{dt_g} \left( t_g^{3n} \frac{dh}{dt_g} \right) = g t_g^{3n} \quad (19)$$

449 Therefore, the  $h(t_g)$  can be written as:

450 
$$h(t_g) = \frac{g t_g^2}{6n + 2} \quad (20)$$

451 At the moment of a bubble's detachment, as is shown in Fig. 13, the bubble is a  
452 flattened spheroid shaped and the  $h(\tau_d)$  can be written in this form:

453 
$$h(t_g) = b \quad (21)$$

454 By analyzing the experimental data, it can be found that the ratio of minor axis and  
455 the major axis is approximately a constant value  $b/a = 0.3$ . Therefore, Eq.(21) can  
456 be rewritten as:

457 
$$h(t_g) = \frac{\sqrt{30}}{10} R_{eq} \quad (22)$$

458 Kim et al[11] pointed out that the bubble radius is proportional to the power of  
459 2/3-1/2 of growth time. According to our experimental data, the parameter n is equal  
460 to 1/2. So the bubble departure diameter is:

461 
$$D_d = \frac{2\sqrt{30}}{15} g t_g^2 \quad (23)$$

#### 462 **3.4.4 Comparison of bubble departure diameters correlations with experimental** 463 **data**

464 The six most commonly used bubble departure diameters correlations were chosen  
465 to compare with the experimental data. As defined in Eq. 24 and 25, the average  
466 deviation (AD) and the absolute average deviation (AAD) are used to evaluate those  
467 correlations. The results are presented in Table 4 and the comparisons between the  
468 experimental and predicted bubble diameters are shown in Fig. 14.

$$469 \quad AD = \frac{1}{N} \sum_1^N \frac{\text{predictedvalue} - \text{experimentalvalue}}{\text{experimentalvalue}} \times 100 \quad (24)$$

$$470 \quad ADD = \frac{1}{N} \sum_1^N \left| \frac{\text{predictedvalue} - \text{experimentalvalue}}{\text{experimentalvalue}} \right| \times 100 \quad (25)$$

471 As is presented in Table 4, Fritz [9] and Cole and Shulman [12] didn't predict well  
 472 in sub-atmospheric pressure, with deviations more than 95% in all of the conditions.  
 473 Cole and Shulman [12] include the bubble growth rate based on Fritz correlation.  
 474 However, due to lack of Jacob number in their correlations, the effect of the system  
 475 pressure is neglected. As a result, their correlations are limited in sub-atmospheric  
 476 conditions. Cole [13] modified Fritz correlation by taking a constant number 0.04  
 477 instead of the contact angle and involving the Jacob number. The data show the trends  
 478 and work reasonably in 20kPa, but in lower pressure large deviations are observed.

479 By integrating three dimensionless numbers  $Ja$ ,  $Pr$  and  $Ar$  into  $K_1$ , the  
 480 correlations proposed by Kuyayeladze and Gogonin [14] and Jensen and Memmel [15]  
 481 were quite similar. The correlation developed by Jensen and Memmel [15] showed  
 482 big deviations in all of the conditions except for 12.3kPa. Kuyayeladze and Gogonin  
 483 [14] agreed well within  $\pm 30\%$  at three conditions (20kPa water, 7.2kPa water and  
 484 7.2kPa  $CaCl_2$  solution). However, in lower pressure (5.6kPa), their correlation was  
 485 not applicable because the dimensionless number  $K_1$  got out of range ( $K_1 > 0.06$ ).  
 486 The correlations proposed by Kim and Kim [16] showed the best results with  
 487 deviations with  $\pm 30\%$  in all of the conditions. Dimensional analysis involving the  
 488 characteristic time scale and characteristic bubble radius scale were used in their  
 489 studies.

490 The comparison between the experimental and Eq.19 is illustrated in Fig. 15a. As  
 491 can be seen from the picture, the new correlation predicted well in all of the  
 492 experimental conditions. The predicted departure diameters of the new correlation  
 493 were within  $\pm 20\%$  deviation, which showed great improvement to predict in  
 494 sub-atmospheric pool boiling conditions.

495 **3.4.5 Comparison of new bubble departure diameter correlation with different**  
 496 **literature data**

497 In this section, a comparison between literature data [2][25][26] and prediction data  
498 that calculated by new correlation was made. Stralen and Cole [2] took water as  
499 working fluid, the working pressure ranges from 4.08kPa to 20.28kPa. While Stralen,  
500 Sluyter and Cole [25] took water, water-ethanol and water-1-butanol as working fluid,  
501 the pressure ranges from 3.6kPa to 6.6kPa. The working fluid of Cole and Shulman's  
502 [26] experiment was water, the pressure was between 6.7kPa and 13kPa. As shown in  
503 Fig. 15b, the new correlation predicts well in most of the experimental conditions,  
504 especially for water(4.08kPa)[2,26] and binary mixtures (3.6kPa-6.6kPa)[26].

#### 505 **4. Conclusions**

506 Nucleate pool boiling experiments of water and calcium chloride solution were  
507 carried out at sub-atmospheric pressure in a range of 3.6kPa to 22.0kPa. A high-speed  
508 camera was used to capture the bubble images. The bubble dynamic parameters were  
509 measured and calculated, the bubble growth curves in different boiling conditions  
510 were obtained. The main conclusions are listed as follows.

511 For distilled water, due to the low vapor density and high surface tension force, the  
512 bubble diameter tends to increase as pressure decreases. Additionally, as the wall  
513 superheat rises, the thermal boundary layer become thicker and results in larger  
514 bubble departure diameters. In sub-cooling conditions, the condensation effect and the  
515 Marangoni flow hinder the bubble growth, resulting in a smaller bubble size. The  
516 experiments of water verified the methods and procedure successfully, and provide  
517 basic data for the new correlation.

518 For calcium chloride solution, a complex boiling regime with irregular bubble  
519 dynamic parameters was observed, comparing to water under the same pressure, the  
520 effect of smaller vapor density outweighs that of the surface tension force, which  
521 results in the decrease in departure frequency and increase in departure diameter.  
522 Moreover, with the increase of concentration, the bubble departure diameter tends to  
523 decrease and frequency tends to increase respectively owing to the smaller vapor  
524 density and stronger Marangoni flow.

525 Finally, based on bubble force balance analysis, the relationship of buoyancy force,  
526 pressure force, the inertial force, the Maragoni force and the surface tension force was  
527 analyzed. Considering sub-atmospheric pressure environment, the inertia force is the  
528 dominant negative force, so after simplification of force balance equation, a new

529 correlation was proposed. The developed correlation can predict the whole data of  
530 distilled water and calcium chloride solution within  $\pm 20\%$  deviation. For the  
531 literature data, the developed correlation has a mean deviation of 17.2% and 6.3% for  
532 water and binary mixtures, respectively.

533

### 534 **Acknowledgments**

535 The research work described in this manuscript was supported by the National  
536 Natural Science Foundation of China (Grant No.51106094) as well as Natural Science  
537 Foundation of Shanghai (Grant No. 16ZR1414700 and 18040501800). Their support  
538 is gratefully acknowledged.

539

### 540 **Reference**

---

[1] R. McGillis, V.P. Carey, J.S. Fitch, W.R. Hamburg, Pool boiling on a small heat dissipating element in water at low pressure, in: ASME/AIChE National Heat Transfer Conference, Minneapolis, Minnesota, 1991.

[2] S.J.D. van Stralen, R. Cole, W.M. Sluyter, M.S. Sohal, Bubble growth rates in nucleate boiling of water at sub-atmospheric pressures, In International Journal of Heat and Mass Transfer, Volume 18, Issue 5, 1975, Pages 655-669, ISSN 0017-9310

[3] S.J.D. Van Stralen, W.M. Sluyter, Local temperature fluctuations in saturated pool boiling of pure liquids and binary mixtures, In International Journal of Heat and Mass Transfer, Volume 12, Issue 2, 1969, Pages 187-198, ISSN 0017-9310.

[4] V.V. Yagov, A.K. Gorodov, D.A. Labuntsov, Experimental study of heat transfer in the boiling of liquids at low pressures under conditions of free motion, J. Eng. Phys. 18 (1970) 421–425.

[5] Florine Giraud, Romuald Rullière, Cyril Toubanc, Marc Clausse, Jocelyn Bonjour, Experimental evidence of a new regime for boiling of water at subatmospheric pressure, In Experimental Thermal and Fluid Science, Volume 60, 2015, Pages 45-53, ISSN 0894-1777.

[6] B. Zajackowski, T. Halon, Z. Krolicki, Experimental verification of heat transfer coefficient for nucleate boiling at sub-atmospheric pressure and small heat fluxes, Heat Mass Transf. 52 (2016) 205–215.

[7] Jeongbae Kim, Cheol Huh, Moo Hwan Kim, On the growth behavior of bubbles during saturated nucleate pool boiling at sub-atmospheric pressure, In International Journal of Heat and Mass Transfer, Volume 50, Issues 17–18, 2007, Pages 3695-3699, ISSN 0017-9310.

[8] Sandra Michaie, Romuald Rullière, Jocelyn Bonjour, Experimental study of bubble dynamics of isolated bubbles in water pool boiling at subatmospheric pressures, In Experimental Thermal and Fluid Science, Volume 87, 2017, Pages 117-128, ISSN 0894-1777.

[9] Fritz W. Maximum volume of vapor bubbles. Phys Z. 1935;36:379–84.

- 
- [10] Cole R, Rohsenow WM. Correlation of bubble departure diameters for boiling of saturated liquids. *Chem Eng Prog Symp Ser* 1969;65(92):211–3.
- [11] Rajiva Lochan Mohanty, Mihir Kumar Das, A critical review on bubble dynamics parameters influencing boiling heat transfer, In *Renewable and Sustainable Energy Reviews*, Volume 78, 2017, Pages 466-494, ISSN 1364-0321, <https://doi.org/10.1016/j.rser.2017.04.092>.
- [12] Cole R, Shulman HL. Bubble departure diameters at sub-atmospheric pressures. *AIChE Chem Symp Ser* 1966;62(64):6–16.
- [13] Cole R. Bubble frequency and departure volumes at sub-atmospheric pressures. *AIChE J* 1967;13:779–83.
- [14] SS. Kutateladze, II. Gogonin, Growth rate and detachment diameter of a vapor bubble in free convection boiling of a saturated liquid, *Teplofizika Vysokikh Temperatur* 17 (1979) 792–797.
- [15] M.K. Jensen, G.J. Memmel, Evaluation of bubble departure diameter correlations, in: *Proceedings of the Eighth International Heat Transfer Conference*, vol. 4, 1986, pp. 1907–1912.
- [16] J. Kim, M.H. Kim, On the departure behaviors of bubble at nucleate pool boiling, *Int. J. Multiph. Flow* 32 (10) (2006) 1269–1286.
- [17] M. Gong, J. Ma, J. Wu, Y. Zhang, Z. Sun, Y. Zhou, Nucleate pool boiling of liquid methane and its natural gas mixtures, *Int. J. Heat Mass Transf.* 52 (11) (2009) 2733–2739.
- [18] John R. Howell and Robert Siegel, Incipience, growth, and detachment of boiling bubbles in saturated water from artificial nucleation site of known geometry and size. Technical paper proposed for presentation at Third International Heat Transfer Conference Chicago, Illinois, August 8- 12, 1966.
- [19] Zuber N, Hydrodynamics aspects of boiling heat transfer, US AEC Report AECU 4439, 1959.
- [20] Qiu DM, Dhir VK, Hasan MM, Chao D, Neumann E, Yee G, Witherow J. Single Bubble Dynamics during Nucleate Boiling under Microgravity Conditions. Engineering foundation Conference on microgravity fluid physics and heat transfer. Honolulu, HI; 1999.
- [21] Dhir VK, Abarajith HS, Li D. Bubble dynamics and heat transfer during pool and flow boiling. *Heat Transf Eng* 2007;28(7):608–24.
- [22] M.S. Plesset, S.A. Zwick, The growth of vapor bubbles in superheated liquid, *J. Appl. Phys.* 25 (1954) 493–500.
- [23] H.K. Forster, N. Zuber, Growth of vapor bubbles in superheated liquid, *J. Appl. Phys.* 25 (1954) 474–478.
- [24] J. Kim, M.H. Kim, On the departure behaviors of bubble at nucleate pool boiling, *Int. J. Multiph. Flow* 32 (10) (2006) 1269–1286.
- [25] S.J.D. Van Stralen, W.M. Sluyter and R.Cole, Bubble growth rates in nucleate boiling of aqueous binary systems at sub-atmospheric pressures, *Int. J. Heat Mass Transfer.* 1975;19:931-941.
- [26] Cole R, Shulman HL, Bubble growth rates at high jakob numbers, *Int. J. Heat Mass Transfer.* 1966;9:1377-1390.

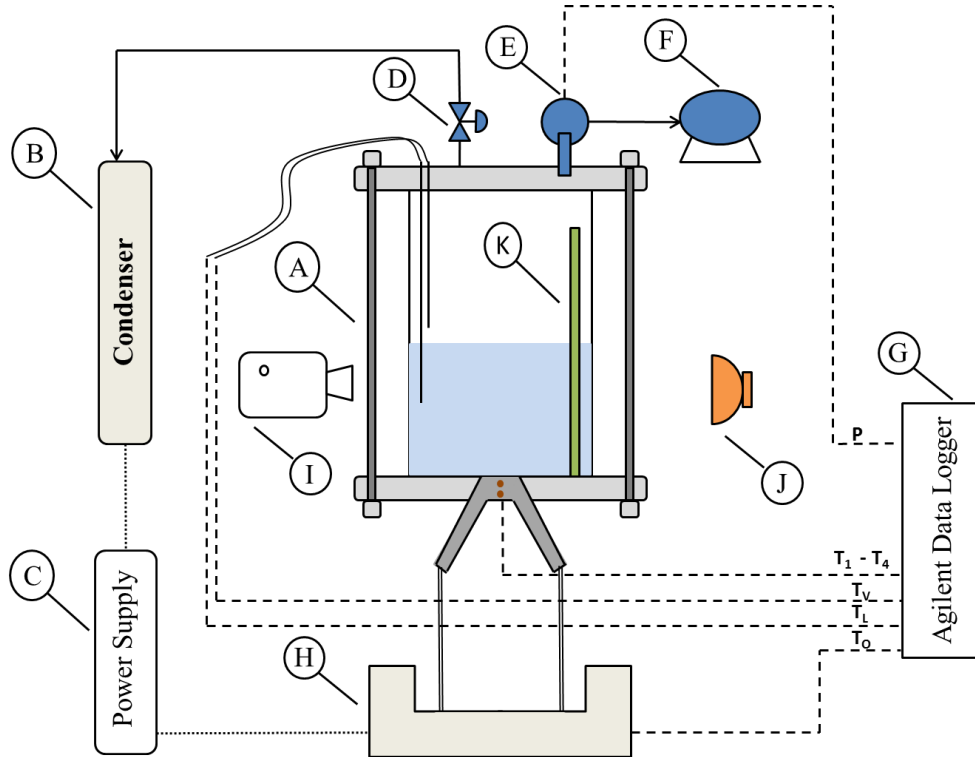


Figure.1. Schematic of the experimental apparatuses. (A) Boiling Vessel; (B) Condenser; (C) Power Supply; (D) Valve; (E) Vacuum Pressure Transducer; (F) Vacuum Pump; (G) Agilent Data Logger; (H) Controlled Oil Bath; (I) High Speed Camera; (J) Halogen Backlight Device; (K) Stainless Steel Ruler

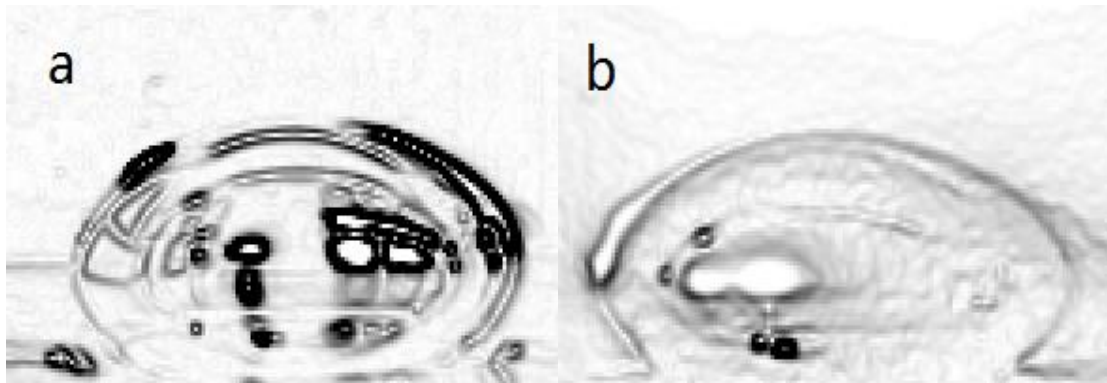


Fig. 2. Processed bubble images of distilled water(a) and calcium chloride aqueous solution(b)  
 $(P_v=20\text{kPa}, H_1=15\text{cm}, T_s=60^\circ\text{C})$



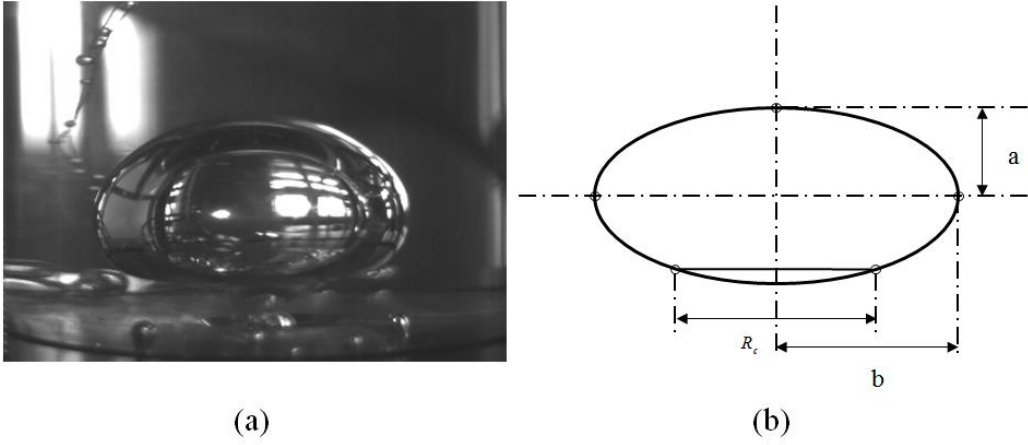


Figure.3 A flattened spheroid shaped bubble (a) and the geometry of a flattened spheroid(b)

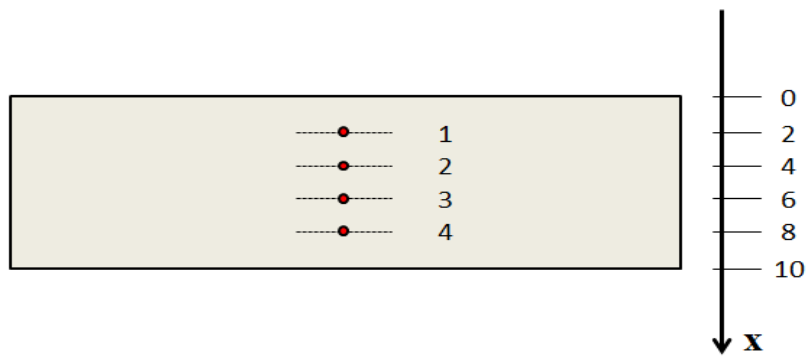


Fig. 4 . Corresponding measurement points schematic diagram

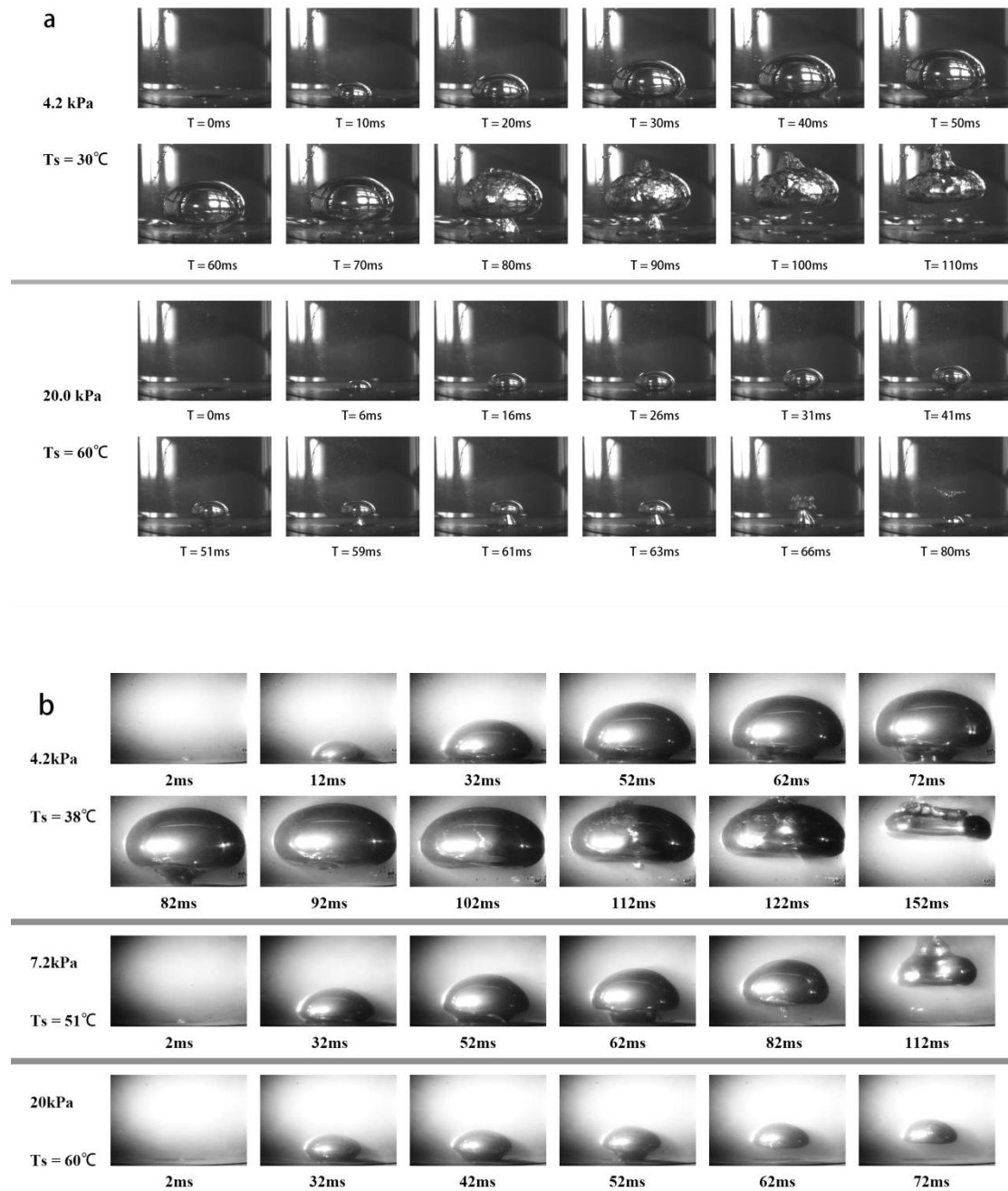
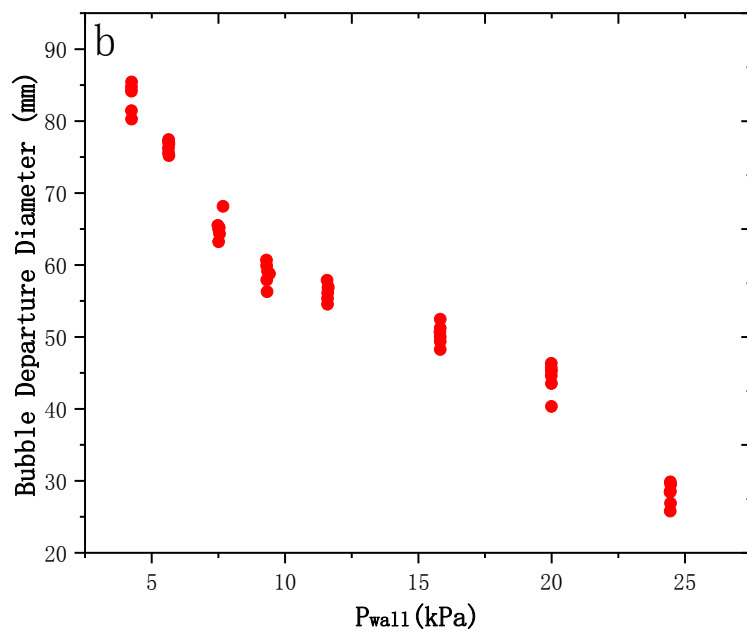
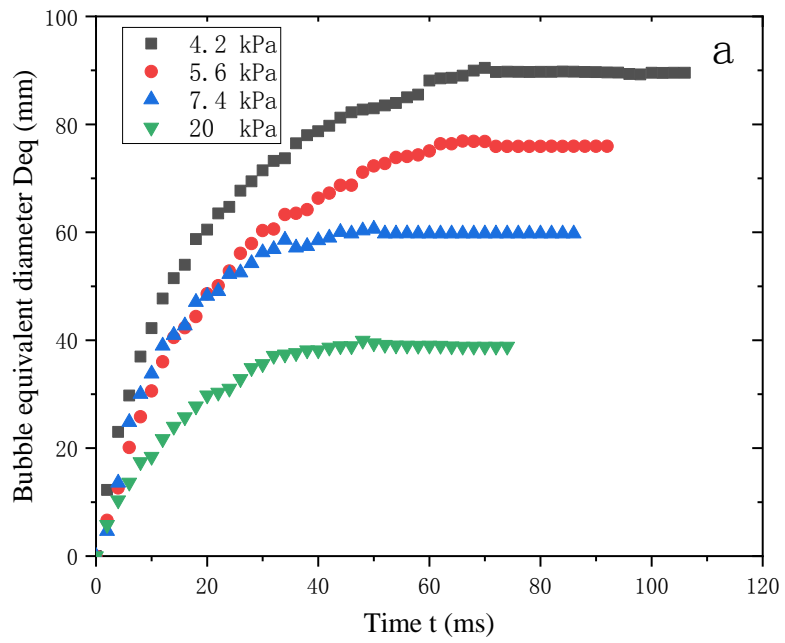
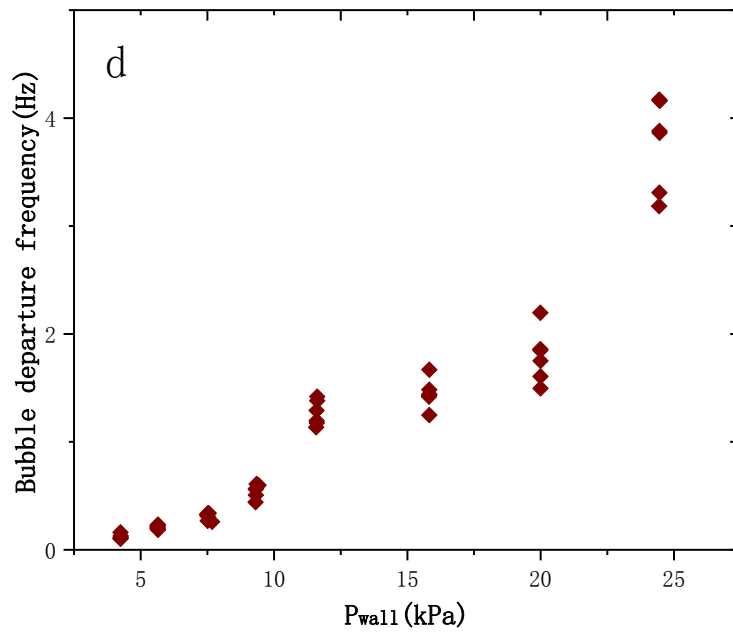
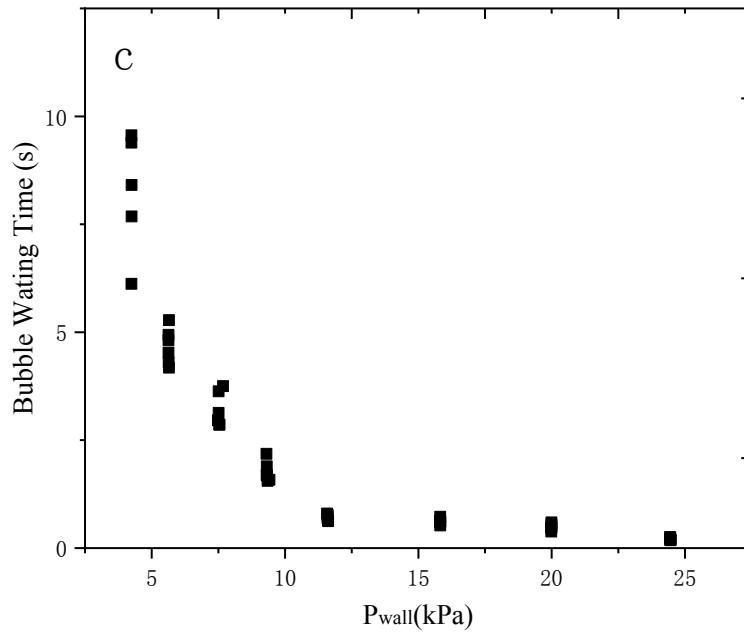
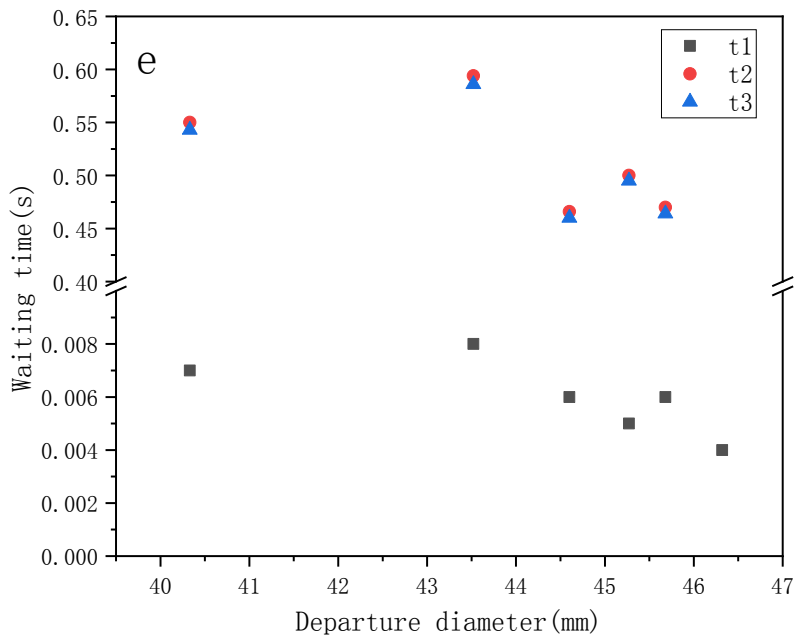


Figure.5. Typical Bubble shape under different pressure (a)(distilled Water,  $H_1 = 15\text{cm}$ ,  $\Delta T = 20\text{K}$ ), (b) (calcium chloride aqueous solution,  $H_1 = 15\text{cm}$ ,  $\Delta T = 20\text{K}$ , wt = 30%)







( Distilled Water,  $H_1 = 15\text{cm}$ ,  $\Delta T = 40\text{K}$ ,  $\Delta T_{\text{sub}} = 0\text{K}$  )

Figure.6. Bubble growth curves(a), bubble departure diameter(b), bubble waiting time(c) and departure frequency(d) at different pressure and bubble waiting time of mushroom shape bubble at 20kPa(e).

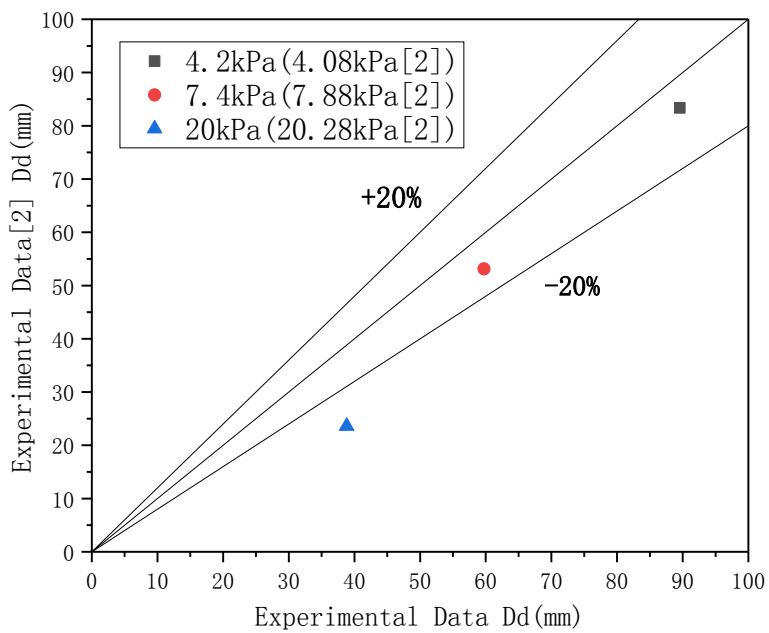


Figure.7. Experimental bubble departure diameter in comparison with literature data[2]

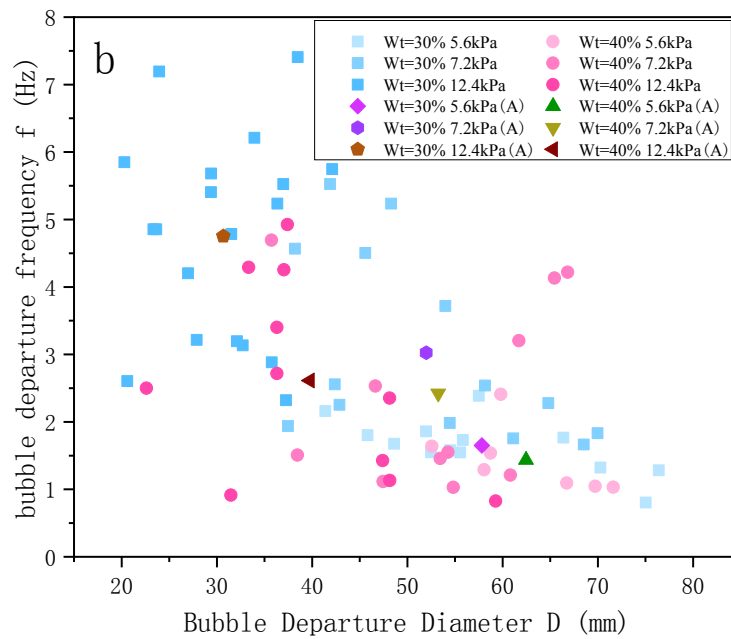
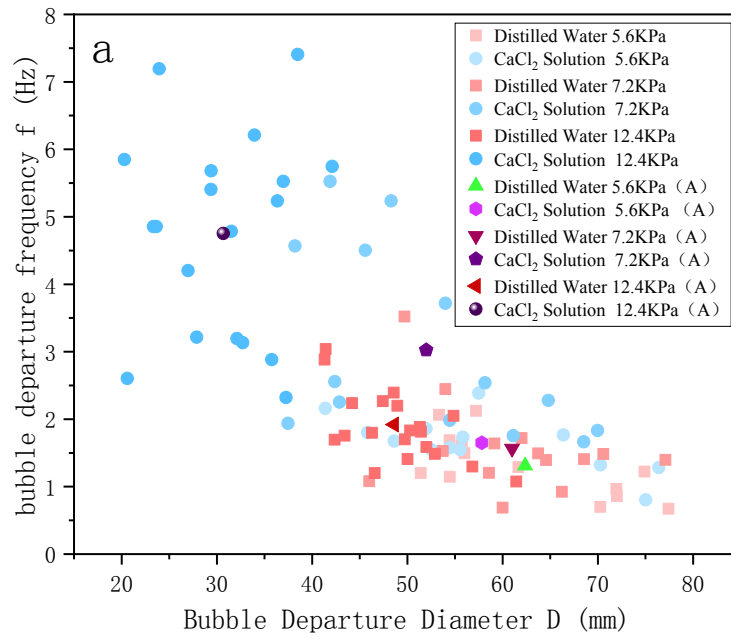


Figure.8. The comparison between distilled water and calcium chloride aqueous solution of bubble departure diameter and frequency in different pressure(A:Average value)(  $H_1 = 15\text{cm}$ ,  $\Delta T = 20\text{K}$ ,  $w_t = 30\%$ )(a) and the bubble departure diameter and frequency in different concentration(A:Average value)(calcium chloride aqueous solution,  $H_1 = 15\text{cm}$ ,  $\Delta T = 20\text{K}$ )(b)

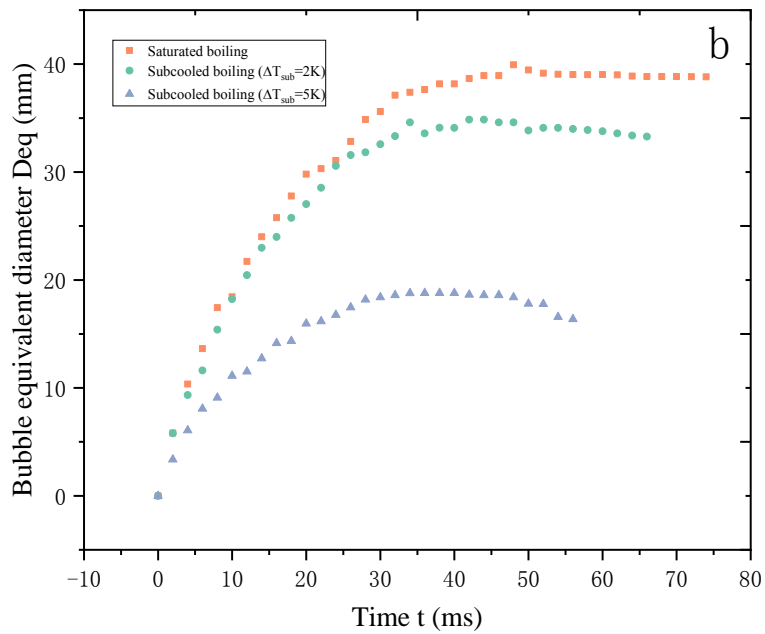
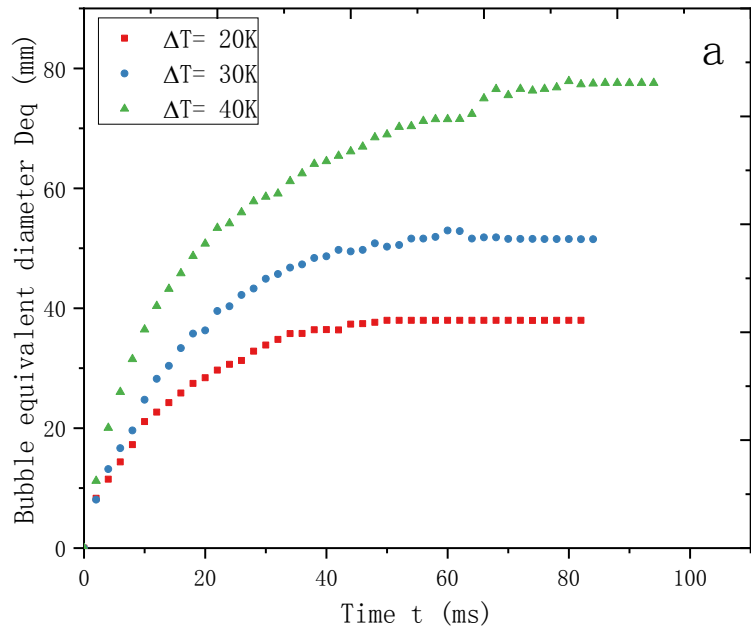


Figure.9. The bubble growth curves under different values of superheat temperature (Distilled Water,  $P = 5.6kPa$ ,  $H_1 = 15cm$ ) (a) and the bubble growth curves in saturated boiling and subcooled boiling (Distilled Water,  $P = 20kPa$ ,  $H_1 = 15cm$ ,  $\Delta T = 30K$ ) (b)

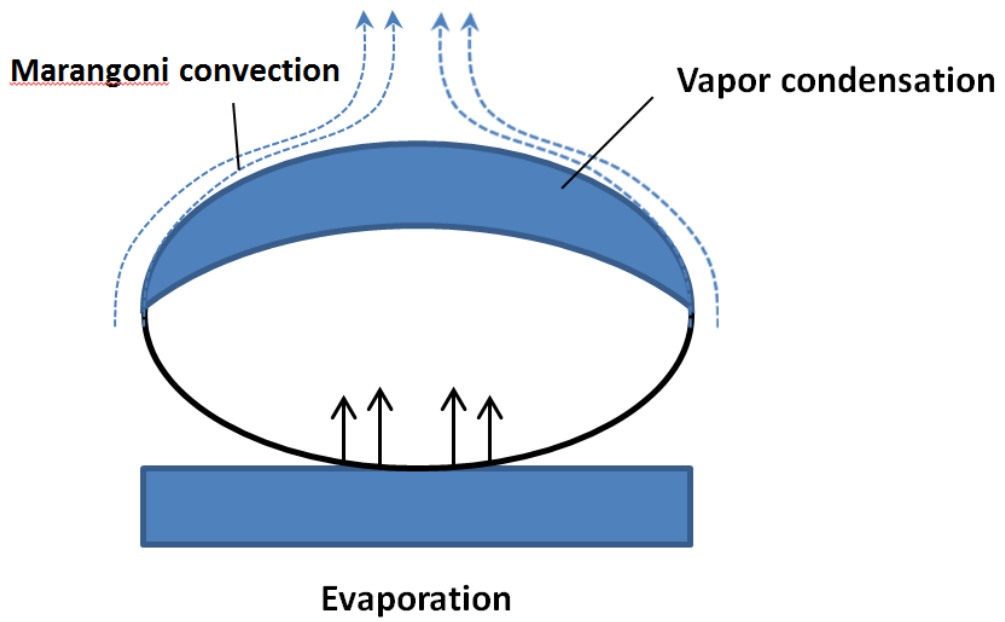
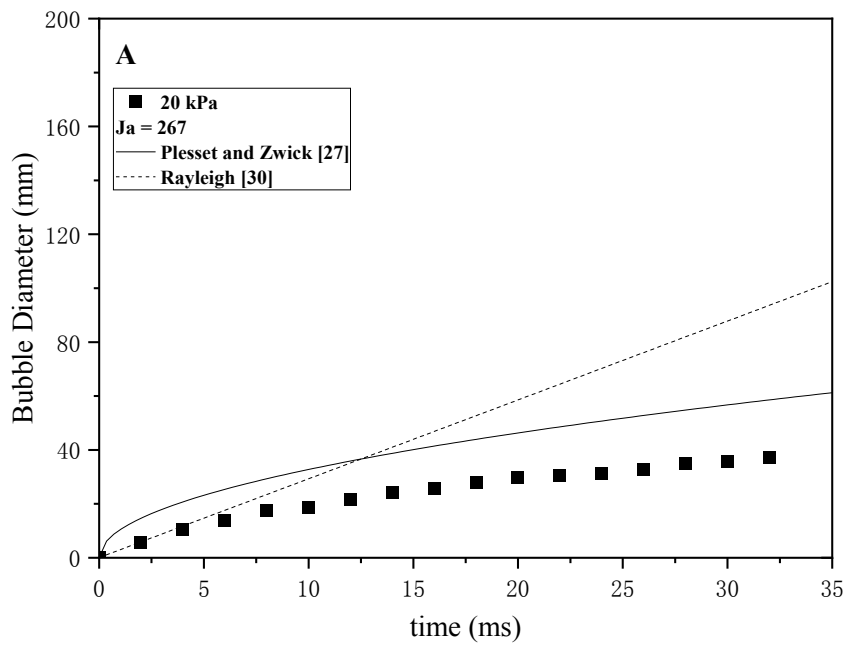


Figure.10. The subcooled boiling mechanism





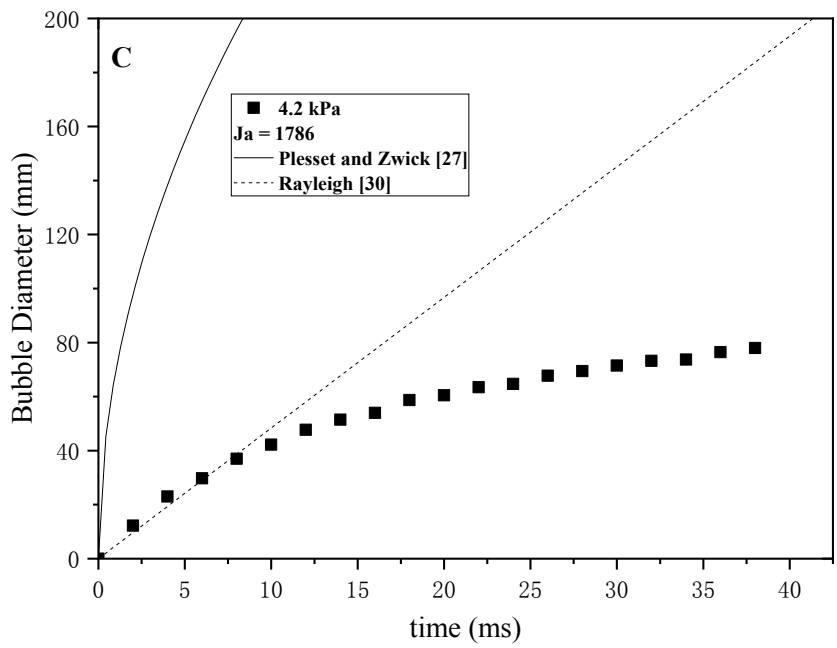
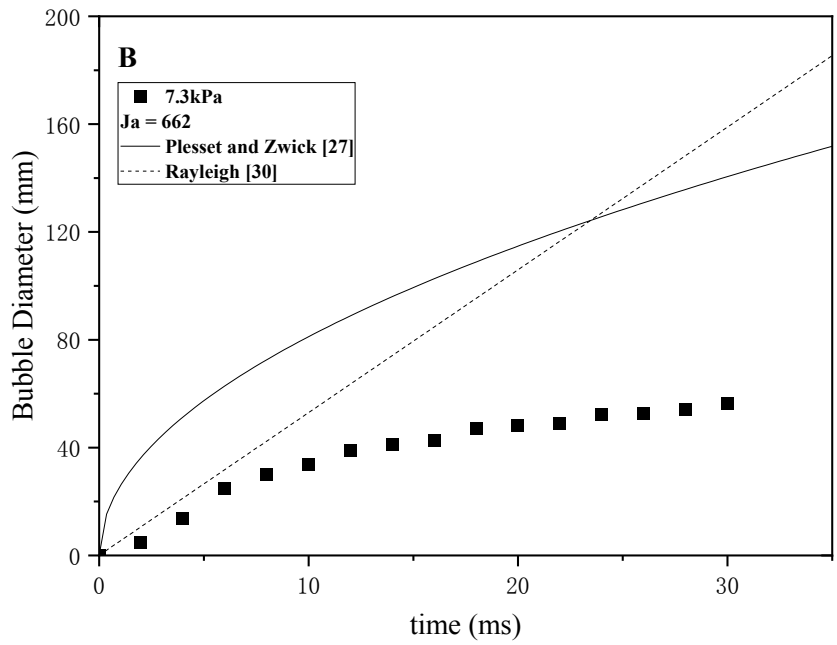
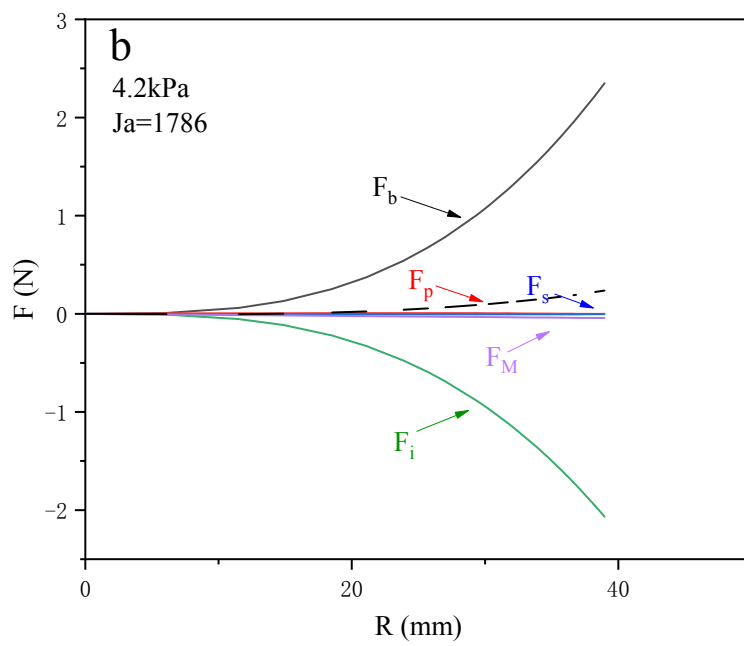
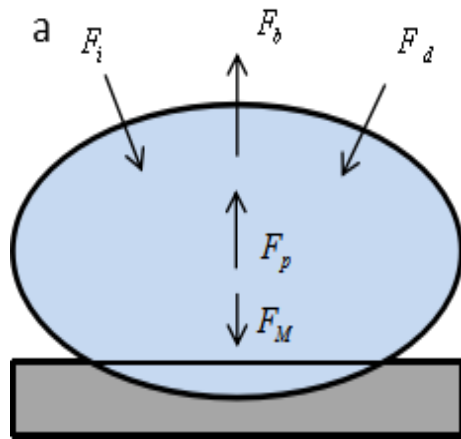


Figure.11. Comparison of the growth rate correlations with experimental data  
(Distilled Water,  $H_1 = 15\text{cm}$ )



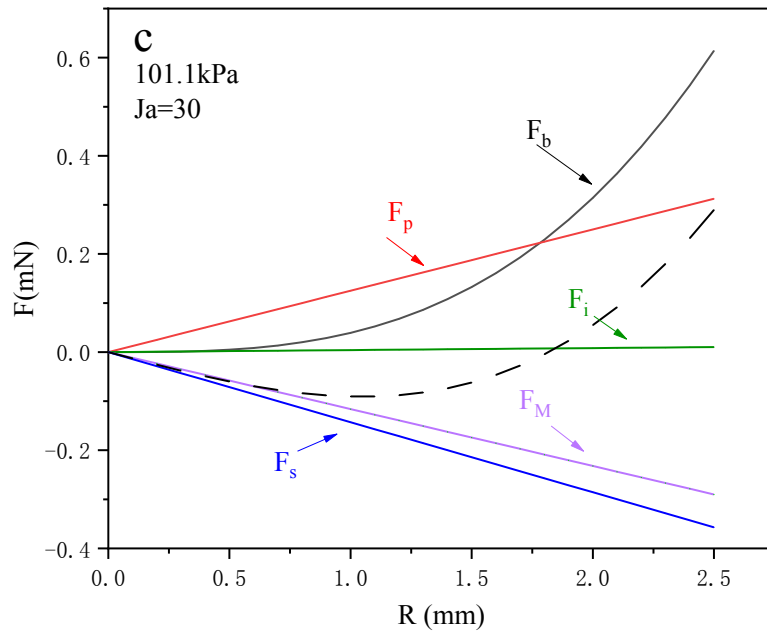


Figure.12. The geometric parameters and force acting on an isolated bubble(a)and the relationship between the forces acting on the isolated bubble and the bubble radius 4.2KPa (b) 101.kPa(c)

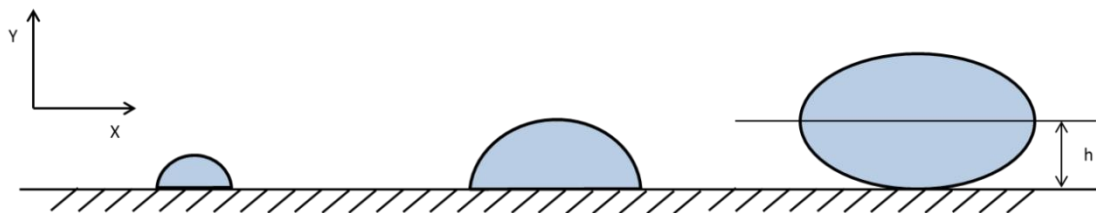
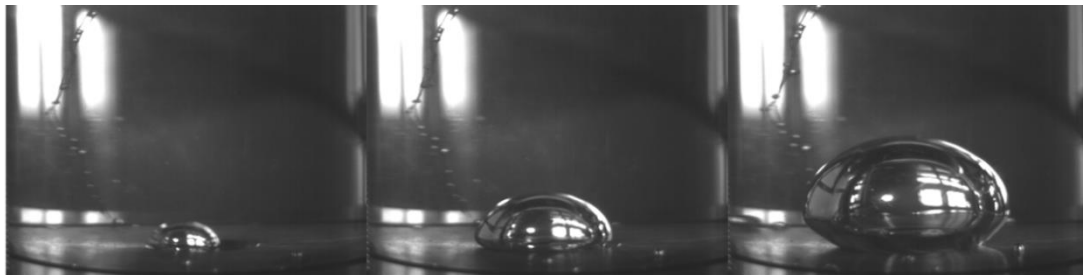
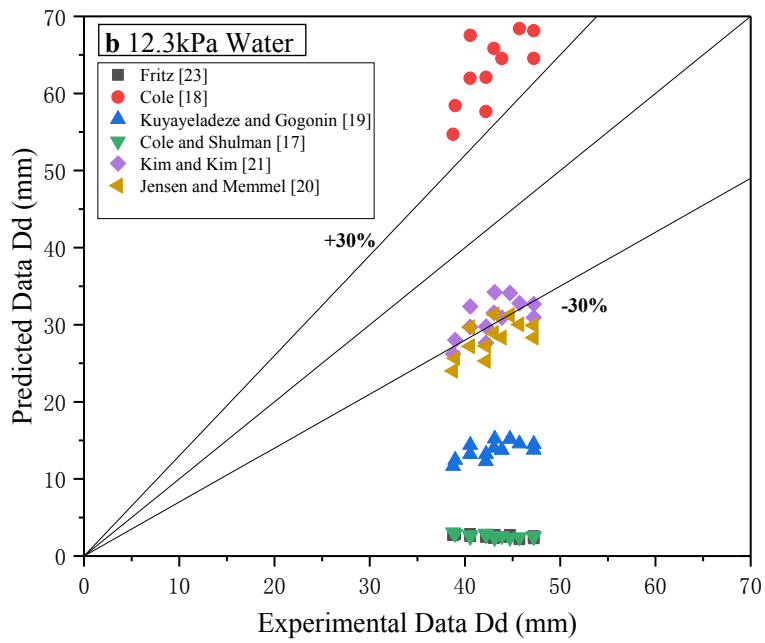
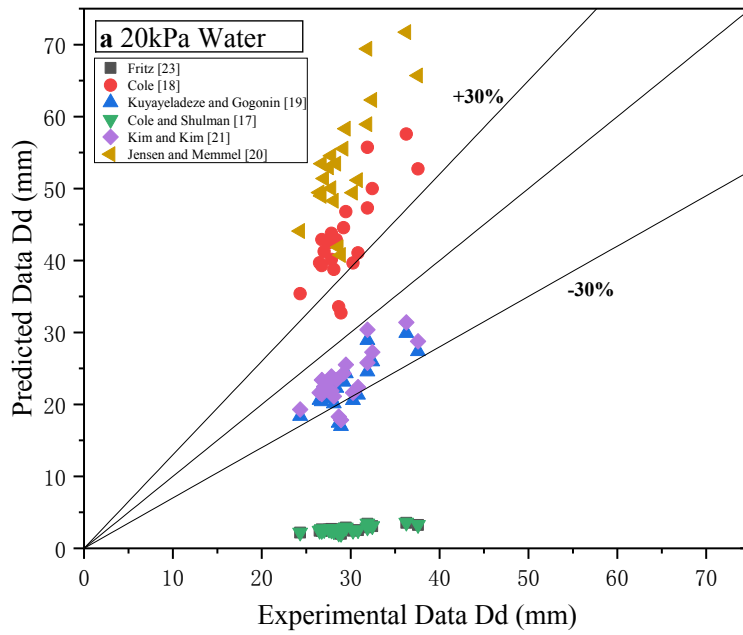
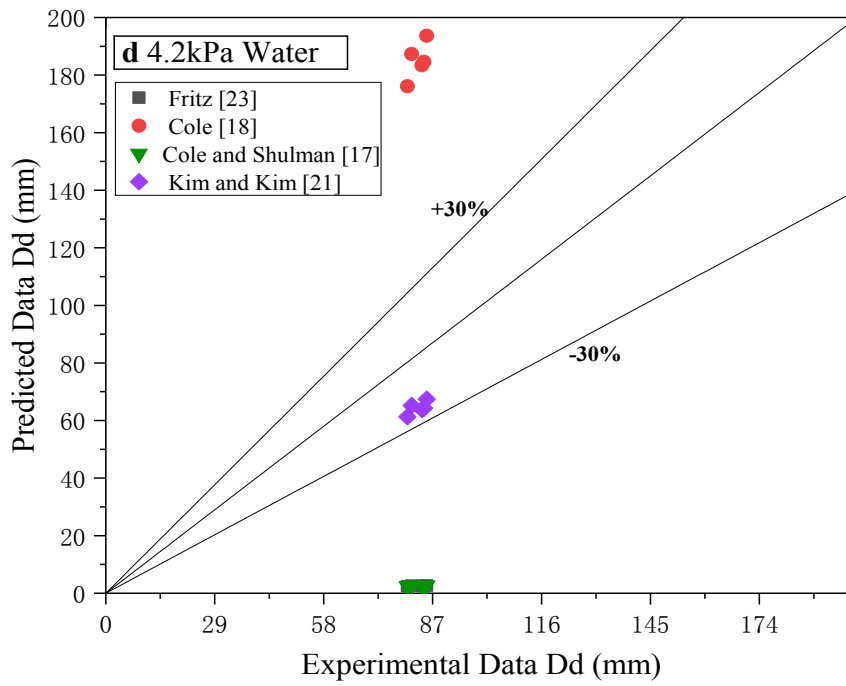
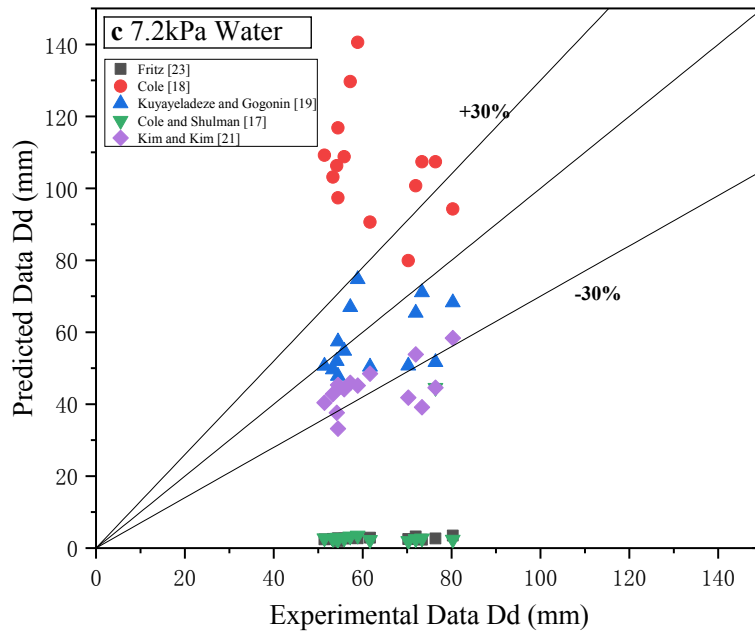


Figure.13. The growth and departure behavior of an isolated bubble under subatmospheric pressure





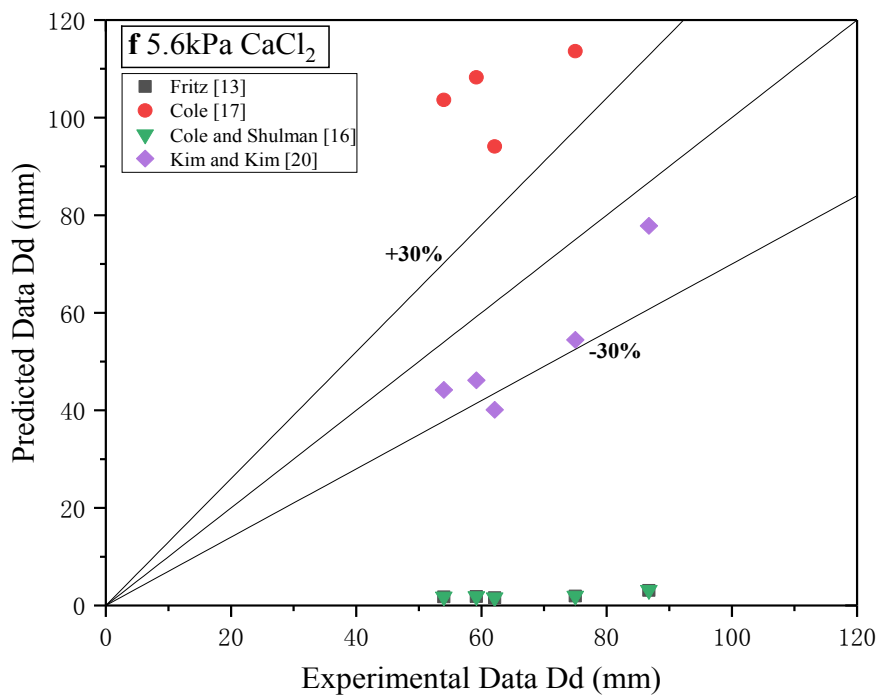
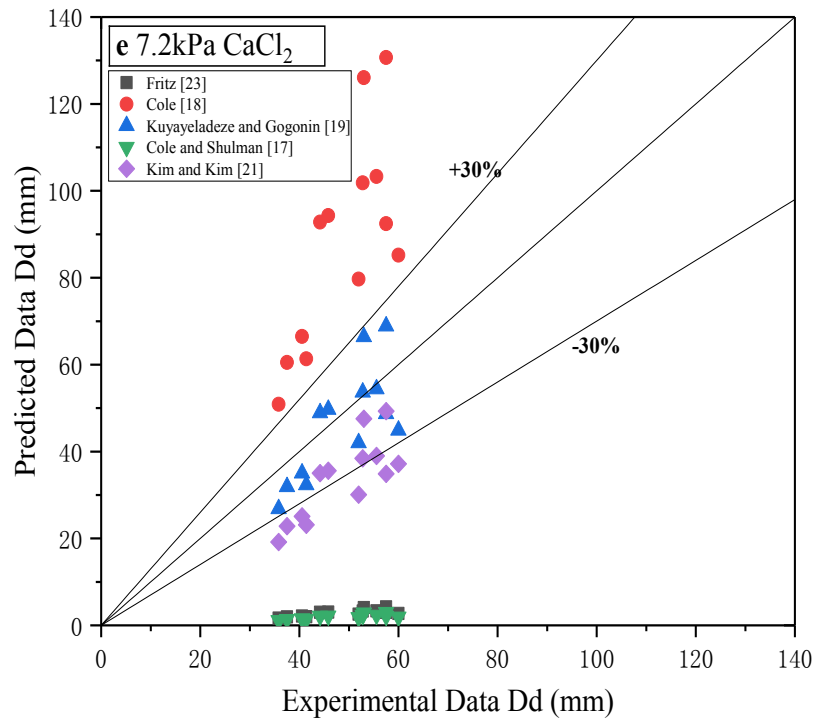


Figure.14. comparisons between the experimental and predicted bubble diameters with different correlations in different operating conditions

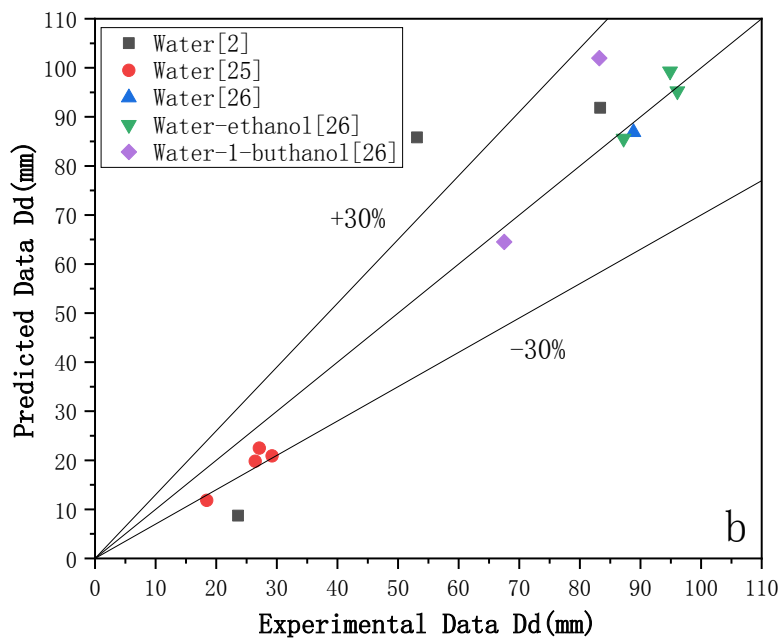
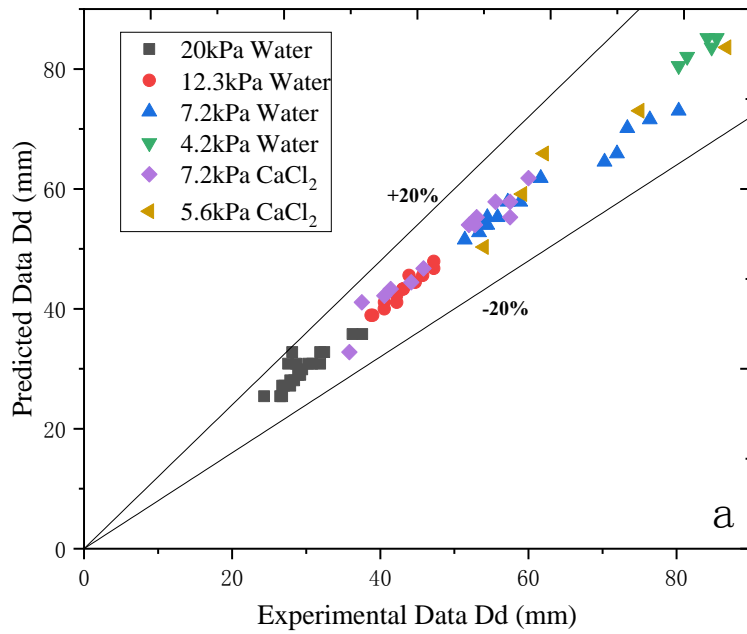


Figure.15. Comparisons between the experimental data and the new bubble departure diameter correlation in different operating conditions(a) and Comparisons of literature data and new bubble departure diameter correlation prediction data(b)





**-able 1**

Bubble departure diameter and frequency correlations

---

$D_d = 0.02080 \left[ \frac{\sigma g_c}{g(\rho_l - \rho_v)} \right]^{1/2} \left[ 1 + 0.0025 \left( \frac{dD}{dt} \right)^{3/2} \right]$	Cole and Shulman[12]
$D_d = 0.04 Ja \left[ \frac{2\sigma}{g(\rho_l - \rho_v)} \right]^{1/2}$	Cole[13]
$D_d = 0.25(1 + 10^5 K_1)^{1/2} \left[ \frac{\sigma g_c}{g(\rho_l - \rho_v)} \right]^{1/2}$	Kutateladeze and Gogonon[14]
For $K_1 < 0.06$ , where $K_1 = \left( \frac{Ja}{Pr_l} \right)^2 (Ar)^{-1}$	
$D_d = 0.19(1.8 + 10^5 K_1)^{2/3} \left[ \frac{\sigma}{g(\rho_l - \rho_v)} \right]^{1/2}$	Jensen and Memmel[15]
$D_d = 0.1649 Ja^{0.7} \left[ \frac{\sigma g_c}{g(\rho_l - \rho_v)} \right]^{1/2}$	Kim and Kim[16]

---

**Table 2**

Uncertainties of the measurement instruments and calculation

---

Parameter	Instrument	Uncertainty
Temperature (K)	K-type thermocouples	$\pm 0.1$ K
Length (mm)	Ruler	$\pm 0.05$ mm
Pressure (kPa)	<a href="#">MD-GA-20K-1-P2-M9-A-T1</a> Absolute pressure transmitter	$\pm 0.2$ kPa
Heat Flux ( $W/cm^2$ )	Omega SA1-T-120	$\pm 8.2\%$
Wall temperature (K)		$\pm 0.1$ K

---

**Table 3**

Operating parameter and physical properties

Wall Superheat	System Pressure		CaCl <sub>2</sub> Concentration	
Range of operating parameter				
0 K – 40 K	3.6kPa – 22 kPa		15 wt% – 40 wt%	
System	Water	Water	Water	CaCl <sub>2</sub> / Water
Pressure	(101.3kPa)	(20kPa)	(4.2kPa)	( 101.3kPa )
T <sub>sat</sub> (°C)	100	60	30	103-110
σ (Nm <sup>-1</sup> )	0.05892	0.06023	0.07118	0.0785-0.0893
c <sub>p</sub> (Jkg <sup>-1</sup> K <sup>-1</sup> )	4,236	4208	4175	2784-3342
K <sub>1</sub> (Wm <sup>-1</sup> k <sup>-1</sup> )	0.679	0.653	0.638	0.554-0.576
ρ <sub>l</sub> (kgm <sup>-3</sup> )	958.4	978.2	998.5	1130-1286
ρ <sub>v</sub> (kgm <sup>-3</sup> )	<b>0.58</b>	<b>0.13</b>	<b>0.03</b>	<b>0.55</b>

**Table 4**

The statistical analysis of the bubble departure diameter at subatmospheric pressures

Pressure (kPa)	Fluid	Correlations	AD	AAD
<b>20</b>	Water	Fritz [13]	-91.037	91.037
		Cole [18]	45.768	45.768
		Kuyayeladze and Gogonin [19]	-24.282	24.282
		Cole and Shulman [17]	-90.941	90.941
		Kim and Kim [21]	-20.513	20.513
		Jensen and Memmel [20]	82.414	82.414
<b>12.3</b>	Water	Fritz [13]	-93.963	93.963
		Cole [18]	50.891	50.891
		Kuyayeladze and Gogonin [19]	-67.833	67.833
		Cole and Shulman [17]	-93.893	93.893
		Kim and Kim [21]	-27.675	27.575
		Jensen and Memmel [20]	-33.768	33.768
<b>7.2</b>	Water	Fritz [13]	-95.812	95.812
		Cole [18]	68.910	68.910
		Kuyayeladze and Gogonin [19]	-18.706	18.706
		Cole and Shulman [17]	-95.751	95.751
		Kim and Kim [21]	-29.858	29.858

4.2	Water	Jensen and Memmel [20]	157.206	157.206
		Fritz [13]	-96.938	96.938
		Cole [18]	122.039	122.039
		Kuyayeladze and Gogonin [19]	/	/
		Cole and Shulman [17]	-96.933	96.933
		Kim and Kim [21]	-22.675	22.675
		Jensen and Memmel [20]	/	/
7.2	CaCl <sub>2</sub> Solution	Fritz [13]	-94.188	94.188
		Cole [18]	79.815	79.815
		Kuyayeladze and Gogonin [19]	-5.263	15.383
		Cole and Shulman [17]	-95.872	95.872
		Kim and Kim [21]	-28.15	32.15
		Jensen and Memmel [20]	192.63	192.63
		Jensen and Memmel [20]	192.63	192.63
5.6	CaCl <sub>2</sub> Solution	Fritz [13]	-97.063	97.063
		Cole [18]	73.54	73.54
		Kuyayeladze and Gogonin [19]	/	/
		Cole and Shulman [17]	-97.002	97.002
		Kim and Kim [21]	-28.34	38.34
		Jensen and Memmel [20]	/	/
		Jensen and Memmel [20]	/	/

---